American Journal of Science

THE MIDDLE ORDOVICIAN TO EARLY SILURIAN VOYAGE OF THE DASHWOODS MICROCONTINENT, WEST NEWFOUNDLAND; BASED ON NEW U/Pb AND ^{40}Ar/^{39}Ar GEOCHRONOLOGICAL, AND KINEMATIC CONSTRAINTS

ARJAN G. BREM*[†], SHOUFA LIN*, CEES R. VAN STAAL**,
DONALD W. DAVIS***, and VICKI J. MCNICOLL****

ABSTRACT. The Dashwoods microcontinent is an important tectonic segment in the peri-Laurentian setting of the Newfoundland Appalachians. In order to better understand the tectonic history of Dashwoods during the Ordovician Taconic orogeny, we have undertaken field mapping, microscopic studies, and U-Pb and ^{40}Ar/^{39}Ar geochronological studies along the northern (Little Grand Lake Fault; LGLF) and western (Baie Verte Brompton Line - Cabot Fault Zone; BCZ) boundaries.

Oblique-dextral ductile deformation in the BCZ occurred from late Middle Ordovician into the Early Silurian, based on the presence of a late syn-tectonic pegmatite dike (455 ± 12 Ma) and a foliated granodiorite sheet (445.8 ± 0.6 Ma). Deformation is coeval with oblique-sinistral accretion along the eastern margin of Dashwoods, which means that Dashwoods and its Notre Dame Arc had a southward translation with respect to the Laurentian margin and the then-present Iapetus Ocean during the Late Ordovician. Dextral movement along the BCZ continued after the collision of Dashwoods with the Laurentian margin. Deformation along the Little Grand Lake Fault is bracketed between 463 ± 5 Ma and 440 ± Ma. These ages combined with other geological arguments indicate that motion probably took place during the Late Ordovician to earliest Silurian contemporaneous with the southward translation of Dashwoods. A possible explanation is that the Snooks Arm arc moved independently from and faster southwards than the Notre Dame Arc with its Dashwoods infrastructure, thereby underthrusting the Dashwoods along the Little Grand Lake Fault.

Our new U-Pb geochronological data, including a muscovite granite (463 ± 5 Ma), a schistose muscovite granite (459 $^{+17}$/$_{-21}$ Ma), and a tectonized tonalite (458 ± 20 Ma), add to the geochronological database of the voluminous second phase of the Notre Dame Arc. Additionally, in all-but-one of our U-Pb samples, inherited grains of Mesoproterozoic (circa 1.0 Ga) age have been obtained. Their regional presence fortifies the possible relationship of the Dashwoods microcontinent with the Long Range Inlier in western Newfoundland. Furthermore, it introduces a potential link with the Blair River Inlier in Cape Breton Island.

INTRODUCTION

The Appalachian - Caledonian mountain chain is a narrow linear mountain belt, the tectonic evolution of which has been compared to the present-day tectonic setting in southwest Pacific Ocean (van Staal and others, 1998). Such mountain chains consist of numerous along-strike segments, including oceanic tracts and microcontinents,

*Department of Earth Sciences, University of Waterloo, Waterloo, Ontario, N2L 3G1, Canada
**Geological Survey of Canada, 601 Booth Street, Ottawa, Ontario, K1A 0E8, Canada
***Department of Geology, University of Toronto, Ontario, M5S 3B1, Canada
****Geological Survey of Canada, 601 Booth Street, Ottawa, Ontario, K1A 0E8, Canada
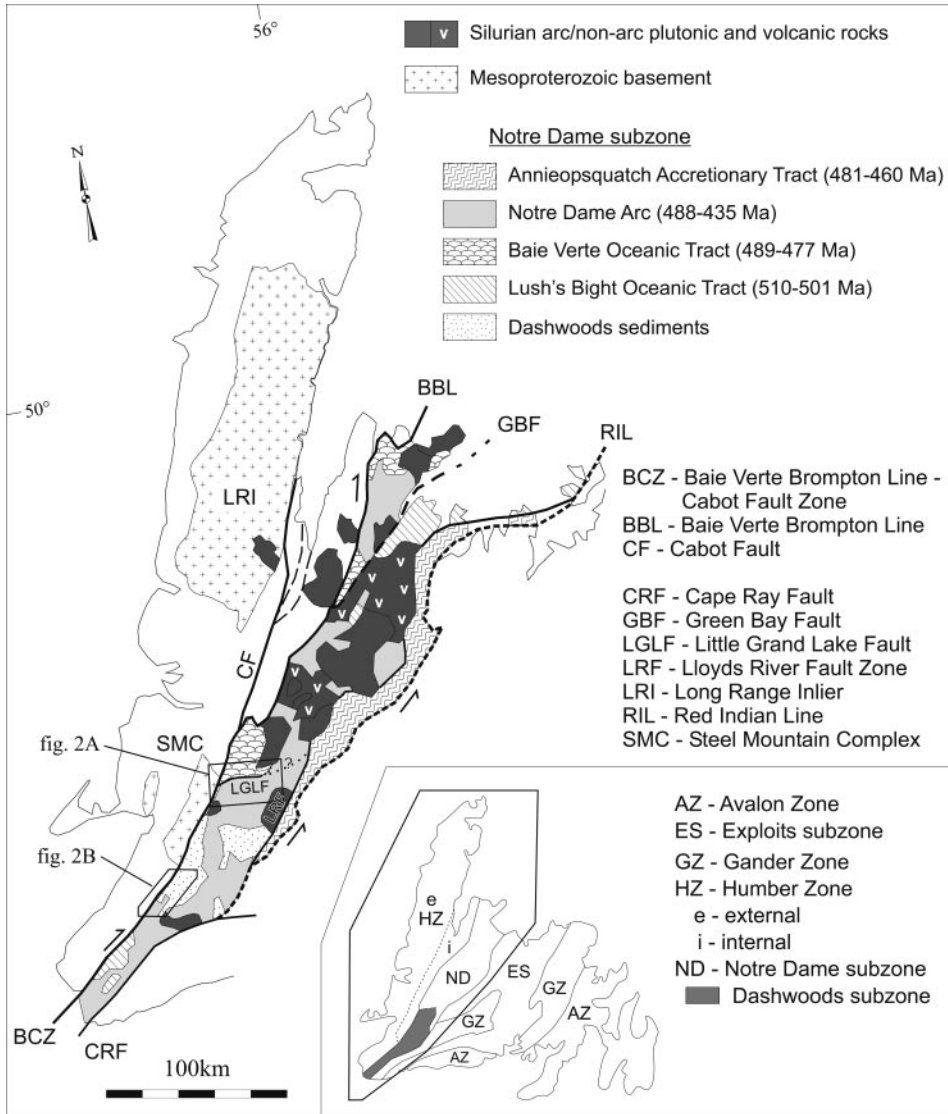[†]Corresponding author: E-mail: agbrem@uwaterloo.ca

Fig. 1. Simplified geological map of western Newfoundland, showing the main tectonic elements discussed in the text (modified after van Staal, 2007). Inset shows the tectono-stratigraphic division of the Newfoundland Appalachians and the position of the Dashwoods subzone (modified after Williams and others, 1988).

each of which has experienced a distinct history. In the western Newfoundland Appalachians, the Notre Dame subzone (Williams and others, 1988) consists of several tectonic segments (fig. 1) that are linked together by their Laurentian affinity and an Ordovician tectono-magmatic event (van Staal, 2007).

The Dashwoods subzone, previously referred to as the Tonalite Terrane (Whalen and Currie, 1983) or Central Gneiss Terrane (Piasecki, 1988; Currie and van Berkel, 1992), represents the southern part of the Notre Dame subzone (fig. 1 inset). It is characterized by the ample presence of metasedimentary rocks, which are scarce in the

northern Notre Dame subzone (fig. 1), and the absence of Early Ordovician oceanic arc rocks, which are present throughout the northern Notre Dame subzone. The Dashwoods subzone has been interpreted as representing a microcontinent (Waldron and van Staal, 2001), which formed the basement to an extensive continental arc (Notre Dame Arc; Whalen and others, 1997) that was intermittently active from Early Ordovician to Early Silurian (489 – 435 Ma; Whalen and others, 1997; van Staal and others, 2007). Collision of Dashwoods with the Laurentian margin during the Middle to Late Ordovician (Taconic orogeny) resulted in regional deformation and high-grade metamorphism, and was followed by late syn- to post-kinematic magmatism and rapid uplift in the Early Silurian (Pehrsson and others, 2003; Whalen and others, 2006).

In order to understand the mosaic of tectonic segments in a mountain belt, it is important to understand the kinematics of boundaries between individual segments. The boundaries of the Dashwoods subzone are all fault zones. The histories of the eastern boundaries of Dashwoods are well documented: The Annieopsquatch Accretionary Tract was accreted to the Dashwoods subzone along the Lloyds River Fault Zone (LRF in fig. 1) in Middle Ordovician (468 – 459 Ma; Lissenberg and others, 2005), and the Cape Ray Fault (CRF in fig. 1) has recorded late Silurian to early Devonian (Acadian) overthrusting of the Dashwoods subzone by high-grade metamorphic rocks of the Gander Zone (Dubé and others, 1996). The northern boundary, the Little Grand Lake Fault (LGLF; fig. 1), is characterized by a marked change in metamorphic grade and has recorded high-angle south-over-north thrusting (Whalen and others, 1993; Piasecki, 1995; Brem and others, 2003). The age of deformation was interpreted as being Middle Ordovician, based on crosscutting relationships, petrographic observations, and regional correlations (Whalen and others, 1993; Piasecki, 1995), but no precise geochronological constraints exist. To the west Dashwoods is separated from the (internal) Humber Zone along the Baie Verte Brompton Line - Cabot Fault Zone (BCZ; fig. 1). The BCZ is a crustal-scale tectonic boundary with a long-lived and complex kinematic history (Wilson, 1962; Hyde and others, 1988; Piasecki and others, 1990; Goodwin and Williams, 1990; van der Velden and others, 2004). Contradicting ductile senses of shear have been reported for the BCZ, and the ages of these ductile movements are poorly constrained. Also, younger (Devonian-Carboniferous) brittle-ductile and brittle movements in the BCZ have overprinted and partly obliterated pre-existing deformation features. Hence, no clear consensus exists on the pre-Devonian tectonic history of the BCZ in southwest Newfoundland.

In order to better understand the tectonic history of the Dashwoods microcontinent and its associated sediments and arc plutons in the Appalachian mountain belt, we attempt to improve the understanding of the kinematic history of its northern (LGLF) and western (BCZ) boundaries. We have conducted detailed field studies and thin section analysis to constrain the kinematics of deformation, and we have used U-Pb (ID-TIMS and SHRIMP) and $^{40}Ar/^{39}Ar$ geochronology on selected samples to constrain the timing of deformation. Our results show that the western, northern and eastern boundaries of Dashwoods were active in Late Ordovician time, but the movements along these tectonic boundaries are difficult to reconcile kinematically with one another. We elaborate on a possible explanation of the latter. We also elaborate on the possible link of the Dashwoods microcontinent with nearby basement inliers.

GEOLOGIC SETTING

Dashwoods Subzone - the Dashwoods Microcontinent

The northern and central-western parts of the Dashwoods subzone, which are the focus of our study (figs. 1 and 2), are dominated by clastic metasediments correlated
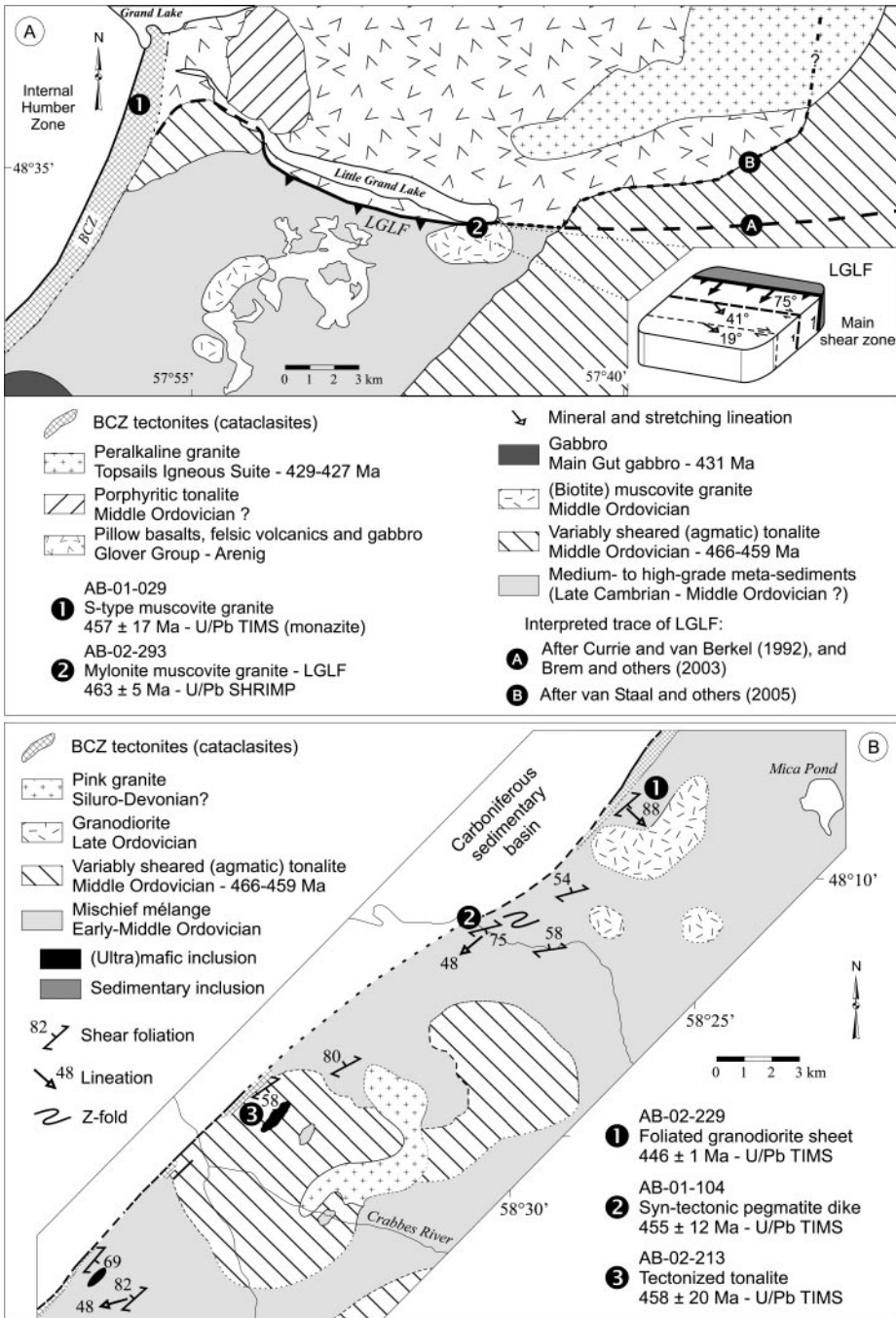
Fig. 2. (A) Simplified geological map of the LGLF region. Numbers indicate the locations of the geochronological samples of this study; letters indicate the proposed traces of the LGLF east of the Little Grand Lake according to different authors as discussed in the text. Inset shows the heterogeneous slip partitioning in the LGLF; (B) Simplified geological map of the central part of the Dashwoods. Numbers indicate the locations of the geochronological samples of this study. See fig. 1 for locations of the areas.

with those of the Mischief Mélange further to the south (Hall and van Staal, 1999), and tentatively correlated with the Fleur de Lys Supergroup in the internal Humber Zone (Hibbard, 1983; Currie and van Berkel, 1992). They include stromatic to nebulitic migmatites, meta-psammitic schist and gneiss, and rare marble and conglomerate layers. Most units contain sillimanite, biotite, muscovite, garnet, and/or hornblende suggestive of medium-to-high grade amphibolite facies metamorphism. However, they also contain retrograde chlorite. Throughout the area, metamorphosed mélange contains various mafic and ultramafic inclusions, which include amphibolite (disrupted mafic dikes?), serpentinized dunite, pyroxenite and gabbro, most of which had been altered prior to incorporation into the mélange (Fox and van Berkel, 1988). The ultramafic inclusions are interpreted as disrupted ophiolitic fragments, and are probably related to the Long Range Mafic-Ultramafic Complex of the southern Dashwoods subzone (Hall and van Staal, 1999).

The metasediments and mélange units have been intruded by voluminous tonalite and granodiorite plutons assigned to the Notre Dame Arc (Whalen and others, 1997), which range in age between 489 to 477 Ma (first phase) and 469 to 459 Ma (second phase) (van Staal and others, 2007; and references therein). These plutons are strongly foliated to non-foliated and most contain xenoliths of (metamorphosed) mafic to ultramafic composition, including amphibolite, gabbro and pyroxenite. In various places, magma mingling of leucocrate granitoid and mafic compositions has occurred (Brem and others, 2003; Pehrsson and others, 2003). On a local, outcrop scale, granodiorite sills are interlayered with the gneissose meta-sediments. Various pegmatite and aplite dikes are present, most of which apparently cut the gneissic fabric, although at least some of these dikes have been caught up in the deformation.

Several plutons of the Notre Dame Arc have yielded xenocrystic components of Mesoproterozoic (1300 – 1650 Ma; for example Dunning and others, 1989; Dubé and others, 1996) and Paleoproterozoic age (circa 2090 Ma; Whalen and others, 1987). Additionally, strongly negative Nd isotopic evidence suggests that the Notre Dame Arc plutons were founded on a continental basement (Whalen and others, 1997). This basement was interpreted to be a microcontinent of Laurentian affinity instead of the leading edge of Laurentia, based on the observation that Dashwoods was obducted by an oceanic tract (the Lush's Bight Oceanic Tract; fig. 1) approximately 20 million years before tectonic loading affected the external Humber Zone (Waldron and van Staal, 2001; van Staal and others, 2007).

Regional deformation and peak metamorphism under amphibolite to lower granulite facies conditions in the Dashwoods subzone are Middle Ordovician (*circa* 460 Ma; for example Dunning and others, 1989; Currie and others, 1992; Pehrsson and others, 2003). This dynamo-thermal event is related to the collision of Dashwoods with the Laurentian margin (van Staal and others, 2007).

Northwestern Notre Dame Subzone - the Baie Verte Oceanic Tract

Rocks immediately north of the LGLF (fig. 1) are part of the Glover Group and consist of mafic (pillow basalts) to silicic (felsic tuffs and rhyolite flows) volcanics, high-level mafic intrusive rocks (mainly gabbro), and sparse sedimentary rocks, including graptolite-bearing Arenig shales (Williams, 1992). These rocks overlie gabbro, trondhjemite, serpentinized peridotites and other mafic to ultramafic rocks of the Glover Island complex (*circa* 490 Ma; Cawood and van Gool, 1998). This complex is interpreted as representing oceanic crust of the Baie Verte Oceanic Tract (van Staal, 2007) that formed in the Humber Seaway, the narrow seaway between the Humber margin and the Dashwoods microcontinent (Waldron and van Staal, 2001). Subsequently, the Baie Verte Oceanic Tract formed the basement to an Early Ordovician oceanic arc / back arc complex (Bédard and others, 2000), which includes the Glover Group.

Regional deformation and (sub-) greenschist metamorphism of these rocks occurred before the Early Silurian (Cawood and van Gool, 1998). They were subsequently intruded by latest Ordovician to Early Silurian granodiorite plutons (for example 440 Ma Glover Island granodiorite; Cawood and van Gool, 1998), and voluminous high-level peralkaline granites (for example 427 – 429 Ma Topsails Igneous suite; Whalen and others, 1987).

In fact, throughout the Notre Dame subzone (including the Dashwoods subzone), latest Ordovician to Early Silurian plutons of felsic (granodiorite to granite) and mafic compositions (gabbro to quartz diorite, diabase) are exposed (figs. 1 and 2; Whalen and others, 2006; and references therein). In outcrop, these units are commonly undeformed and unmetamorphosed (for example, *circa* 431 Ma Main Gut gabbro; Dunning and others, 1989). Some intrusions truncate the strong regional fabric developed in the metasediments of the Dashwoods as well as plutons of earlier phases of the Notre Dame Arc.

(Internal) Humber Zone - Humber Margin of the Laurentian Continent

The units west of the BCZ form part of the Humber Zone, which is interpreted as the Laurentian margin (Williams, 1995). The Humber Zone was divided into an external and an internal zone based on a difference in metamorphic grade and style of deformation (fig. 1; Cawood and others, 1994). In southwestern Newfoundland, the internal Humber Zone is characterized by a Proterozoic (?) anorthosite complex that is structurally overlain by Late Neoproterozoic crystalline basement and associated – mainly clastic – metasediments. Regional deformation and peak metamorphism (up to amphibolite facies conditions) of the latter units occurred in the Early Silurian (*circa* 430 Ma; Salinic orogeny; Cawood and others, 1994), 30 million years after peak metamorphism and deformation in the Dashwoods subzone. Evidence for large-scale Ordovician (Taconic) deformation, metamorphism and plutonism in the internal Humber Zone is absent (Brem, 2007). However, some Taconic influence is expected, since the stratigraphic record in the external Humber Zone clearly suggests that the Humber margin was being loaded in the Middle Ordovician (Williams, 1995). The difference in age and style of deformation and metamorphism between the Dashwoods subzone and internal Humber Zone shows that these segments were not juxtaposed until after the Early Silurian (Cawood and van Gool, 1998; Brem, 2007).

DASHWOODS BOUNDARIES - OBSERVATIONS AND INTERPRETATIONS

BCZ - Western Dashwoods Subzone Boundary

General.—In southwestern Newfoundland the Carboniferous Cabot Fault Zone (Wilson, 1962) coincides with the Ordovician Baie Verte Brompton Line (Williams and St-Julien, 1982) and separates the Dashwoods subzone of the western Dunnage Zone from the Humber Zone (BCZ in fig. 1; Williams and St-Julien, 1982; Williams, 1995); hence the BCZ is a long-lived crustal-scale tectonic zone with a very complex kinematic history (Wilson, 1962; Hyde and others, 1988; Goodwin and Williams, 1990; Brem and others, 2002; van der Velden and others, 2004). In southwestern Newfoundland, the BCZ is also referred to as the Long Range Fault (for example Piasecki and others, 1990; Currie and van Berkel, 1992). The generally wide tectonic zone consists of anastomosing ductile and brittle-ductile shear zones that are crosscut and overprinted by intense high-level brittle-ductile and brittle structures. As a result, most pre-existing ductile deformation features have been obliterated. Moreover, rocks caught up in the BCZ have been deformed to the extent that in most places positive identification of a protolith is not possible. However, the brittle overprint is concentrated in a narrow zone along the present-day Humber Zone - Dunnage Zone boundary (fig. 2), and the older ductile fabrics away from this zone are relatively undisturbed.
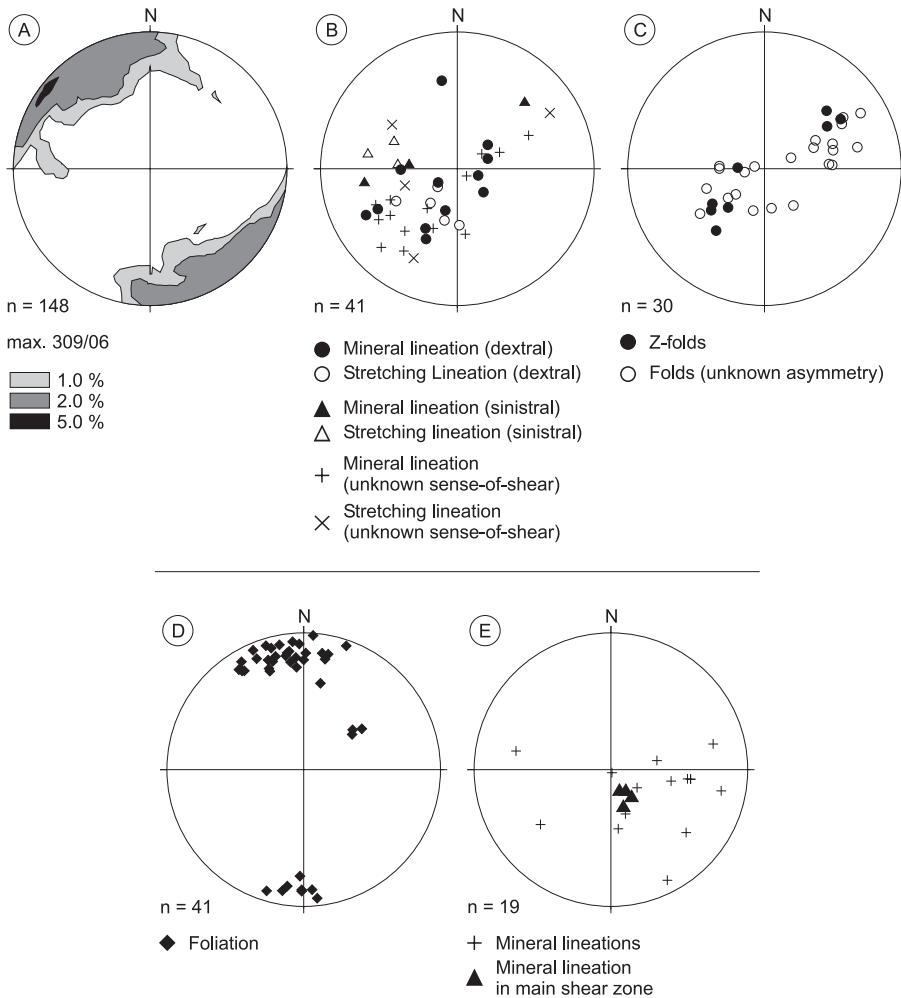
Fig. 3. Equal-area lower-hemisphere projections of: (A) Contours of poles to foliation of the high-strain fabric of the BCZ; (B) lineations associated with the high-strain fabric of the BCZ; (C) fold axes of asymmetric folds in the BCZ; (D) poles to foliation in the LGLF; and (E) mineral and stretching lineations in the LGLF.

Internal geometry and kinematics of the BCZ.—The western part of the Dashwoods subzone is characterized by gneissic to migmatitic metasediments and variably foliated igneous units. The gneissic foliation and localized high-strain zones are steeply dipping and generally strike NE (orogen parallel), but deviations from this direction to northerly and easterly strikes occur (fig. 3A). In the gneissic rocks, the foliation is planar and defined by quartz-feldspar plates and biotite and/or hornblende-rich layers. In areas of lower strain, where individual marble and conglomerate layers could be identified, the foliation has developed parallel to sedimentary layering. In migmatites and high-strain zones, the foliation is commonly curvi-planar and irregular (fig. 4A).

Stretching lineations, defined by elongate quartz-feldspar aggregates, and mineral lineations defined by biotite and/or hornblende, vary in orientation, but dominantly plunge moderately to steeply towards the southwest (fig. 3B). Shear-sense indicators,
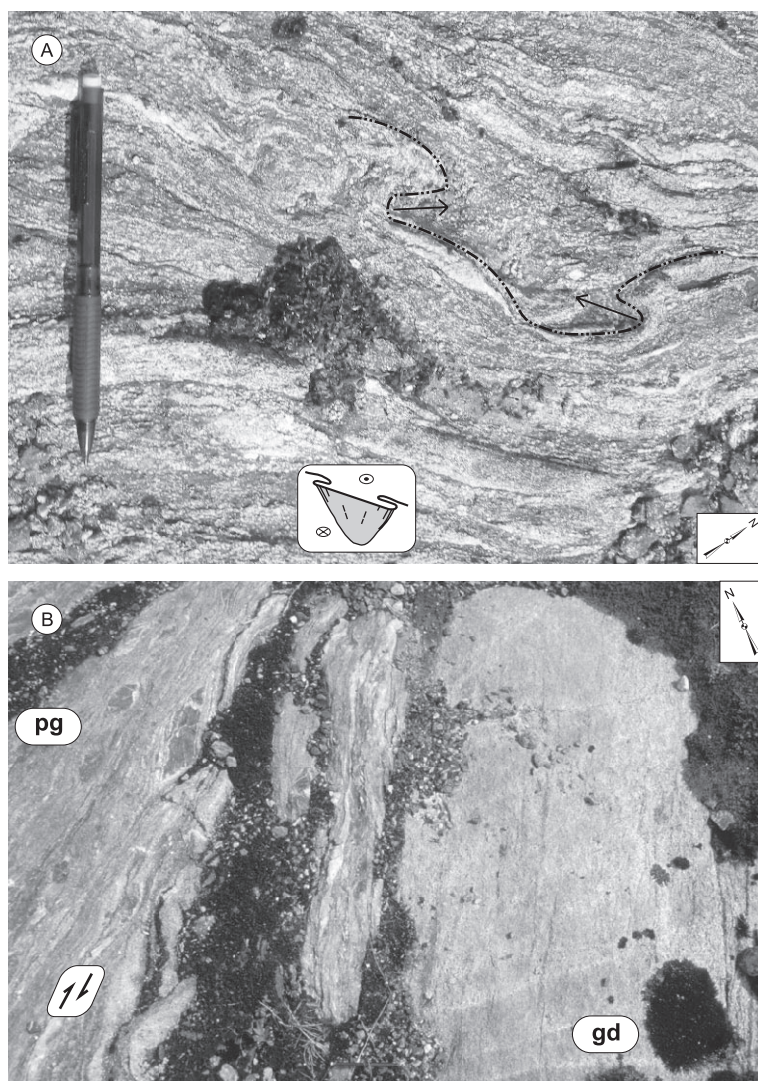
Fig. 4. (A) Sheath fold in high-strain zone developed in paragneiss, with vertical foliation, down-dip mineral lineation, northeast plunging Z-fold axis and southwest plunging S-fold-axis. Such geometry is indicative of a northwest-side-up movement; (B) High-strain fabric in xenolith-bearing paragneisses (pg) intruded by xenolith-free granodiorite sheet (gd). Xenoliths in paragneiss show dextral sense of shear. Granodiorite was sampled for U-Pb geochronology (sample AB-02-229). Width of view is approximately 3 meters.

such as sheath folds (fig. 4A), winged objects (fig. 4B), and S-C structures (Passchier and Trouw, 1996) associated with these lineations indicate a prominent dip-slip to oblique-dextral and southeast-side-down movement. This dextral sense of shear is corroborated by Z-folds related to open-to-tight asymmetric folding of the mylonitic foliation (fig. 3C). Thus, the Dashwoods subzone moved down and towards the southwest (in present-day reference frame) with respect to the rocks of the adjacent Humber Zone.

Sinistral shear-sense indicators have also been observed, but these are relatively rare, and less pronounced than the dextral shear-sense indicators. Lineations associ-

ated with the sinistral shear-sense indicators plunge moderately towards the west, whereas the dominant dextral lineations plunge towards the southwest (fig. 3B). Sinistral movement may have post-dated the main dextral shearing, as observed in one outcrop, where a pegmatite dike that truncates the gneissosity was sinistrally offset. This interpretation agrees with the one made by Piasecki (1988). Our preferred interpretation is that sinistral shearing was synchronous with the predominant dextral shearing. Jiang and White (1995; Case III) demonstrated that within a host shear zone, such as the BCZ, locally induced spin may have been strong enough to induce a sense of non-coaxiality, which resulted in antithetic (here sinistral) shear fabrics that are at low angle to the main dextral shear zone.

Syn-kinematic pegmatite dikes.—As described above, the dominant sense of shear observed along the western boundary of the Dashwoods subzone is oblique-dextral. At an outcrop in close proximity to the BCZ (location 2 in fig. 2B) the mylonitic foliation was truncated by a conjugate set of pink pegmatite dikes (fig. 5A). The pegmatite dike that is anti-clockwise from the foliation is stretched and boudinaged, whereas the dike oriented clockwise from the foliation is shortened and folded. Such geometry is indicative of a dextral sense of shear (fig. 5A inset). The dikes intruded the mylonitic foliation either in between two deformational phases (inter-kinematic), or during the latest increments of continuous deformation (late syn-kinematic). Also at the outcrop, several lithologically similar pegmatite dikes truncate the mylonitic foliation but appear undeformed. If these undeformed pegmatite dikes were emplaced at the same time as the deformed dikes, it can be concluded that deformation occurred during
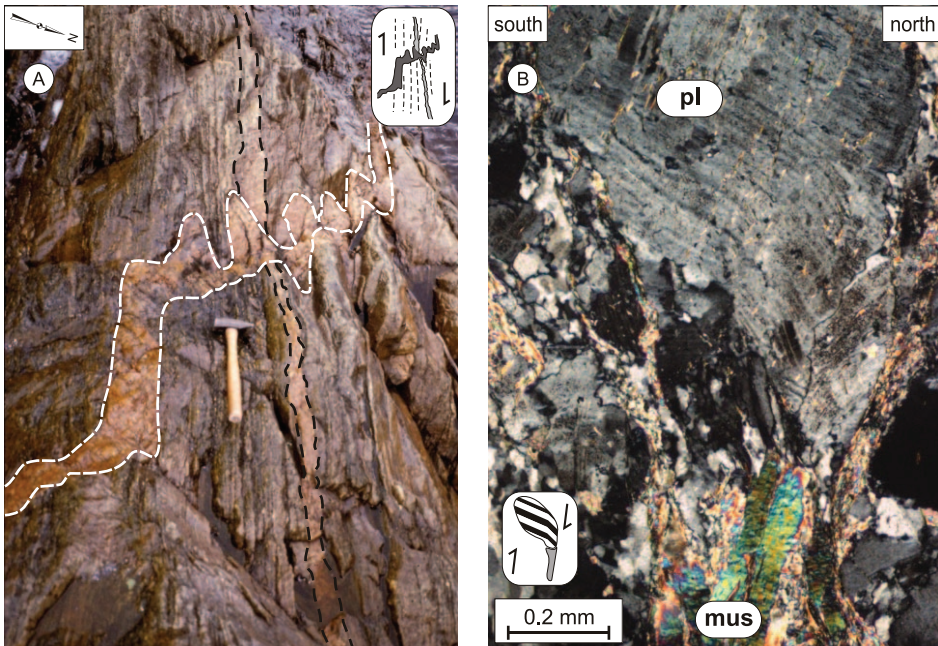

Fig. 5. (A) Field photograph of pegmatite dikes intruding mylonitic paragneisses. The dike clockwise from the foliation is folded (white dashed lines), and the one counter-clockwise from the foliation is boudinaged (black dashed lines). Such geometry is indicative of a dextral sense of shear. The folded vein was sampled for U-Pb geochronology (sample AB-01-104); (B) Photomicrograph of a deformed grain in the main strand of the Little Grand Lake Fault; Plagioclase (pl) porphyroclast with muscovite (mus) tail, indicative of a south-side-up component of movement. Thin section is perpendicular to the foliation and parallel to the down-dip mineral lineation.

pegmatite emplacement. Since deformation of the paragneisses appears to be relatively homogeneous, the deformed pegmatite dikes are interpreted to have intruded during the latest stages of progressive deformation (syn-tectonic). Either way, these deformed dikes constrain the minimum age on the main phase of ductile deformation in the BCZ. The folded pegmatite dike (fig. 5A) was sampled for U-Pb TIMS geochronology (see below).

LGLF - Northern Dashwoods Subzone Boundary

General.—The Little Grand Lake Fault (LGLF) is an east-west trending narrow belt of ductile shear zones that marks a distinct metamorphic break between the low-grade volcanics to the north and the high-grade meta-sediments to the south (fig. 2A), although this jump in metamorphic grade is absent east of Little Grand Lake (Piasecki and others, 1990; Whalen and others, 1993; Brem and others, 2003). Previously, the LGLF was interpreted to have experienced two deformational events (Piasecki, 1995). However, our work shows that later brittle deformation on low-angle north-dipping thrust planes is merely spatially coincident with part of the trace of the LGLF and is not developed in the LGLF itself. We therefore conclude that the LGLF only experienced one deformational event.

The eastern continuation of the LGLF east of Little Grand Lake is not well constrained. The LGLF was previously thought to curve anti-clockwise towards the Lloyds River Fault Zone (fig. 1; 'A' in fig. 2A; Currie and van Berkel, 1992; Brem and others, 2003). Recently, van Staal and others (2007) proposed that the LGLF takes a northward swing immediately east of Little Grand Lake and appears to hook up with the Green Bay Fault on the north coast of Newfoundland, thereby separating the Baie Verte Oceanic Tract from the Dashwoods subzone - Notre Dame Arc (fig. 1; 'B' in fig. 2A). Due to lack of outcrop east of the Little Grand Lake and overprinting by younger intrusive units, such as the Topsails Igneous Suite, these hypotheses cannot easily be tested. Towards the west, the LGLF is truncated by the BCZ and hence, its continuation west of this lineament could not be established (figs. 1 and 2A).

Internal geometry and kinematics of the LGLF.—The LGLF is best observed in granitoid rocks at the eastern end of Little Grand Lake (fig. 2A; Whalen and others, 1993; Brem and others, 2003), where several strands of the LGLF are exposed, the main strand (at least 40 m wide) being closest to the lake. Towards the south away from the main strand, mylonitic shear zones become sparser and narrower. The shear-related foliation on all strands is steeply south-dipping to vertical (fig. 3D). Mineral lineations, defined by muscovite grains, and stretching lineations, defined by quartz-feldspar aggregates, plunge down dip on the main strand, but towards the south, away from the main shear zone, these plunge shallowly towards the east (fig. 2A inset and fig. 3E).

Shear-sense indicators associated with these fabrics include S-C fabrics, shear bands, bookshelf-stacking and winged objects (fig. 5B; Passchier and Trouw, 1996), and consistently show a reverse to dextral-reverse, south-side up movement. This sense of shear corroborates the observations and interpretation by Whalen and others (1993) and Piasecki (1995), and facilitates the juxtaposition of the high-grade amphibolite facies Dashwoods metasedimentary rocks to the south with greenschist facies volcanic rocks of the Glover Group to the north of the fault. Fault motion thus at least in part must have occurred post peak metamorphism in the Dashwoods metasedimentary rocks.

Microscopic observations and temperature condition of deformation.—The muscovite grains, which define the mylonitic foliation, are both deformed (kinked, bent and fractured) as well as undeformed (fig. 5B), suggesting that muscovite growth was predominantly syn-kinematic, but that some grains may be remnant pre-kinematic grains. In thin section, subgrain domains and undulose extinction characterize the

quartz aggregates. These aggregates are surrounded by numerous small, dynamically recrystallized quartz grains giving the fabric a seriate-interlobate texture (page 46 in Passchier and Trouw, 1996). Feldspar grains are of variable composition, and form characteristic porphyroclasts (fig. 5B) of various sizes, and are commonly internally fractured. Different intracrystalline deformation features have developed in feldspar grains, including undulose extinction, kinks and deformation twins in plagioclase, and perthite exsolution structures in K-feldspar. More importantly, a core-mantle texture defined by subgrain rotation and small, recrystallized feldspars arond larger feldspar clasts is common throughout the thin section (Regime 2 of Hirth and Tullis, 1992). Dynamic recrystallization of quartz may start at temperatures above 300°C (Passchier and Trouw, 1996; Hirth and others, 2001), but recrystallization of feldspar starts to become important at low-to-medium grade conditions (>350°C; Pryer, 1993; Passchier and Trouw, 1996). This would suggest that deformation on the LGLF occurred at greenschist facies conditions or higher, that is probably at temperature conditions near or above the muscovite closure temperature for argon (*circa* 350°C; McDougall and Harrison, 1999).

<div align="center">GEOCHRONOLOGY</div>

<div align="center">*Analytical Procedures*</div>

This is a summary of the analytical techniques of U-Pb ID-TIMS and SHRIMP, and ^{40}Ar/^{39}Ar geochronology. Detailed descriptions of the analytical procedures can be found in the Appendix. Single whole grain zircon and monazite U-Pb analyses were performed at the Jack Satterly Laboratory, University of Toronto (formerly at the Royal Ontario Museum). Standard mineral separation techniques were followed, including methods described by Krogh, 1973, 1982). Data were calculated, regressed and plotted using in-house software (UtilAge by D. W. Davis) with regression based on Davis (1982). Results are presented in table 1 and in figures 6 and 7A. U-Pb SHRIMP II analyses were conducted at the Geological Survey of Canada (GSC) in Ottawa using analytical procedures described by Stern (1997), with standards and U-Pb calibration methods following Stern and Amelin (2003). Results are presented in table 2 and in figure 7B, using Isoplot v. 2.49 (Ludwig, 2001). Laser ^{40}Ar/^{39}Ar step-heating analyses were also performed at the GSC. Data collection protocols of Villeneuve and MacIntyre (1997) and Villeneuve and others (2000) were followed. Error analysis procedures are outlined in Roddick (1988) and Scaillet (2000). Results are presented in table 3 and figures 7C and 7D. All age errors are given at the 95 percent confidence interval.

<div align="center">*Sample Description and Results*</div>

Muscovite granite (AB-01-029).—This K-feldspar-rich, schistose muscovite granite is exposed as a small body in a gully west of Little Grand Lake. None of its contacts are exposed, but these are assumed to be tectonic given its position within the cataclastic zone of the BCZ (fig. 2A). Previously, this unit was interpreted to be part of a muscovite-bearing phase of the Late Neoproterozoic Hare Hill Complex of the Humber Zone (Currie and van Berkel, 1992), but given its unique lithology, we tentatively assign this unit to the Dashwoods subzone.

Ample zircon was obtained from this sample, and two distinct populations were observed: a population of well-rounded brownish grains with pitted surfaces; and a euhedral population of variable morphology, from slender elongate and prismatic grains to short stubby grains and fragments, most of which contain round or rod-shaped inclusions. Five fractions of zircon grains were analyzed, yielding various ^{207}Pb/^{206}Pb ages between 1128 and 1191 Ma (euhedral population) and one older age of 1462 Ma (grain A3; rounded population; table 1; fig. 6A). Back-scattered SEM-imaging shows that zircon grains from the euhedral population have small overgrowths

TABLE 1

U-Pb ID-TIMS isotopic data for zircon and monazite from granitoid rocks of the Dashwoods Subzone, western Newfoundland

No.	Description	Wt. (mg)	U (ppm)	Th/U	Pbtot (pg)	PbCom (pg)	$\frac{206Pb}{204Pb}$	$\frac{206Pb}{238U}$	$\frac{207Pb}{235U}$	$\frac{206Pb}{238U}$ age (Ma)	2σ	$\frac{207Pb}{235U}$	2σ	$\frac{207Pb}{206Pb}$	2σ	Disc %	Error Corr. Coeff.	Lab No.
A	**AB-01-029 schistose muscovite granite, Cabot Fault Zone (UTM 53843-4288)**																	
1	Abr zr, euh, 1 bubble incl	15	85.5	0.42	254.1	1.99	7913.2	0.1887	2.0134	1114.6	3.1	1120.1	2.2	1130.7	3.4	1.5	0.8499	dwd4078
2	Abr zr, euh, clr, rod incl	7.7	166.3	0.77	274.2	0.90	17397.0	0.1900	2.0243	1121.3	2.6	1123.7	1.9	1128.4	2.1	0.7	0.9290	dwd4079
3	Abr zr, rnd, clr, no incl	14	118.7	0.34	404.0	0.80	31550.3	0.2407	3.0443	1390.2	2.9	1418.8	2.0	1462.1	1.6	5.5	0.9507	dwd4080
4	Abr zr, euh, clr, no incl	12	91.4	0.33	214.7	0.76	17948.5	0.1932	2.0680	1138.8	3.2	1138.3	2.3	1137.3	2.2	-0.1	0.9416	dwd4102
5	Abr zr, euh, clr, 1 rod incl	12	29.4	0.26	71.3	0.89	5176.9	0.2030	2.2313	1191.2	3.4	1190.9	2.7	1190.4	4.0	-0.1	0.8592	dwd4103
6	Mon, frag, clr, cracked	4	643.2	19.36	1188.4	27.51	447.5	0.0741	0.5743	461.0	1.1	460.8	7.3	459.9	42.4	-0.2	0.2675	dwd4114
7	Mon, ylw, equant, clr, 1 white incl	10	65.8	40.40	627.7	7.99	446.7	0.0809	0.6560	501.7	1.5	512.2	10.6	559.5	53.5	10.7	0.6677	dwd4115
8	Mon, rnd, ylw, clr, pitted, *	11	21.1	48.56	344.2	2.95	560.8	0.1062	0.9616	650.6	2.2	684.1	9.2	796.0	35.2	19.2	0.5489	dwd4760
9	Mon, ang, ylw, clr, pitted, *	5.9	15.5	41.68	74.4	2.69	163.1	0.0663	0.4940	413.9	2.5	407.6	28.8	372.5	184.0	-11.5	0.8887	dwd4761
B	**AB-01-104 late syn-tectonic pegmatite dike, Dashwoods Subzone (UTM 53342-3872)**																	
10	Abr zr, best pick, **	1.8	355.5	0.22	72.7	0.72	6667.1	0.1165	1.0825	710.3	1.8	744.8	1.7	850.2	3.7	17.4	0.8393	dwd4084
11	Abr zr, 2nd best, **	3.1	490.3	0.35	188.3	0.97	12327.5	0.1225	1.1567	744.8	3.9	780.4	3.1	883.5	3.2	16.6	0.9617	dwd4085
12	Abr zr, bubble incl, crack	3.5	326.2	0.30	153.5	9.35	1073.8	0.1348	1.3047	815.1	1.9	847.8	5.1	934.4	16.0	13.6	0.5507	dwd4086
13	Abr zr, frag, melt incl, **	1.4	376.4	0.24	58.5	0.66	5832.6	0.1131	1.0443	690.9	1.7	726.0	1.7	836.0	3.9	18.3	0.8347	dwd4106
14	Abr zr, clr, equant, melt incl, **	3.1	195.7	0.27	87.9	0.87	6547.8	0.1463	1.4399	880.2	3.3	905.7	2.6	968.3	5.0	9.7	0.8308	dwd4107
C	**AB-02-213 tectonized tonalite, Dashwoods Subzone (UTM 53278-3792)**																	
15	Abr zr, stubby, best pick, **	2.9	362.2	0.27	139.6	1.71	5314.0	0.1343	1.2794	812.6	2.5	836.6	2.1	900.7	5.1	10.4	0.7536	dwd4730
16	Abr zr, **	2.5	269.1	0.36	81.0	1.15	4479.0	0.1189	1.1139	724.2	2.7	760.1	2.3	867.1	6.4	17.4	0.7221	dwd4731
17	Abr zr, rnd, 2nd choice	4.1	171.6	0.33	78.1	2.82	1785.6	0.1105	1.0112	675.8	1.8	709.5	3.1	817.4	10.7	18.2	0.5575	dwd4732
18	Abr zr tip, clr, rnd, **	0.9	389.7	0.27	47.2	0.87	3526.1	0.1358	1.3169	820.9	2.2	853.1	2.3	938.1	5.8	13.3	0.6949	dwd4757
19	Abr zr tip, fuzzy, rnd, crack, **	2.2	192.1	0.36	61.2	1.12	3464.0	0.1425	1.3949	858.7	2.7	886.8	2.5	957.5	5.9	11.0	0.7297	dwd4758
20	Abr zr, frag, rnd, clr, dented, **	2.4	183.9	0.35	63.2	1.23	3284.2	0.1415	1.3742	853.1	2.2	878.0	2.3	941.2	6.0	10.0	0.6829	dwd4759

TABLE 1
(*continued*)

No.	Description	Wt. (mg)	U (ppm)	Th/U	Pbtot (pg)	PbCom (pg)	$\frac{206Pb}{204Pb}$	$\frac{206Pb}{238U}$	$\frac{207Pb}{235U}$	$\frac{206Pb}{238U}$	2σ	$\frac{207Pb}{235U}$	2σ	$\frac{207Pb}{206Pb}$	2σ	Disc %	Error Corr. Coeff.	Lab No.
												age (Ma)						
D	**AB-02-229 foliated granodiorite sheet, Dashwoods Subzone (UTM 53387-3937)**																	
21	Abr zr, needle, multi incl	5.8	140.9	0.65	63.4	9.20	426.6	0.0717	0.5515	446.3	1.4	446.0	10.0	444.3	57.9	-0.5	0.6275	dwd4733
22	Abr zr,	1.6	168.8	0.53	20.3	1.55	818.8	0.0715	0.5508	445.5	1.0	445.5	5.3	445.8	30.0	0.1	0.5545	dwd4734
23	Abr zr, 2nd choice, rnd, clr, **	1.9	98.0	0.53	14.0	2.71	333.9	0.0717	0.5545	446.3	1.3	447.9	12.8	456.6	73.6	2.3	0.7972	dwd4735
E	**AB-02-293 mylonitic muscovite granite, Little Grand Lake Fault (UTM 53784-4443)**																	
24	Abr zr, equant, clr	6.1	207.2	0.41	97.5	3.06	2024.0	0.0757	0.5991	470.4	1.0	476.6	2.8	506.7	14.2	7.4	0.5042	dwd4391
25	Abr zr, equant, opq, bubble incl, **	2.7	261.1	0.26	94.5	24.36	232.2	0.1154	1.0782	704.0	2.8	742.8	16.5	861.4	63.3	19.3	0.2872	dwd4393

UTM measurements are in NAD-27 coordinates
abr = abraded, ang = angular, clr = clear, euh = euhedral, frag = fragment, incl = inclusion, mon = monazite, opq = opaque, rnd = round, ylw = yellow; zr = zircon
* = before dissolution, grain was treated with HNO_3 to remove the hematite (?) coating from the grains
** = no column chemistry (Krogh, 1973) performed on zircons
PbCom is common Pb, assuming the isotopic composition of laboratory blank
Th/U calculated from radiogenic $^{208}Pb/^{206}Pb$ ratio and $^{207}Pb/^{206}Pb$ age assuming concordance
% Disc., is per cent discordance for the given $^{207}Pb/^{206}Pb$ age
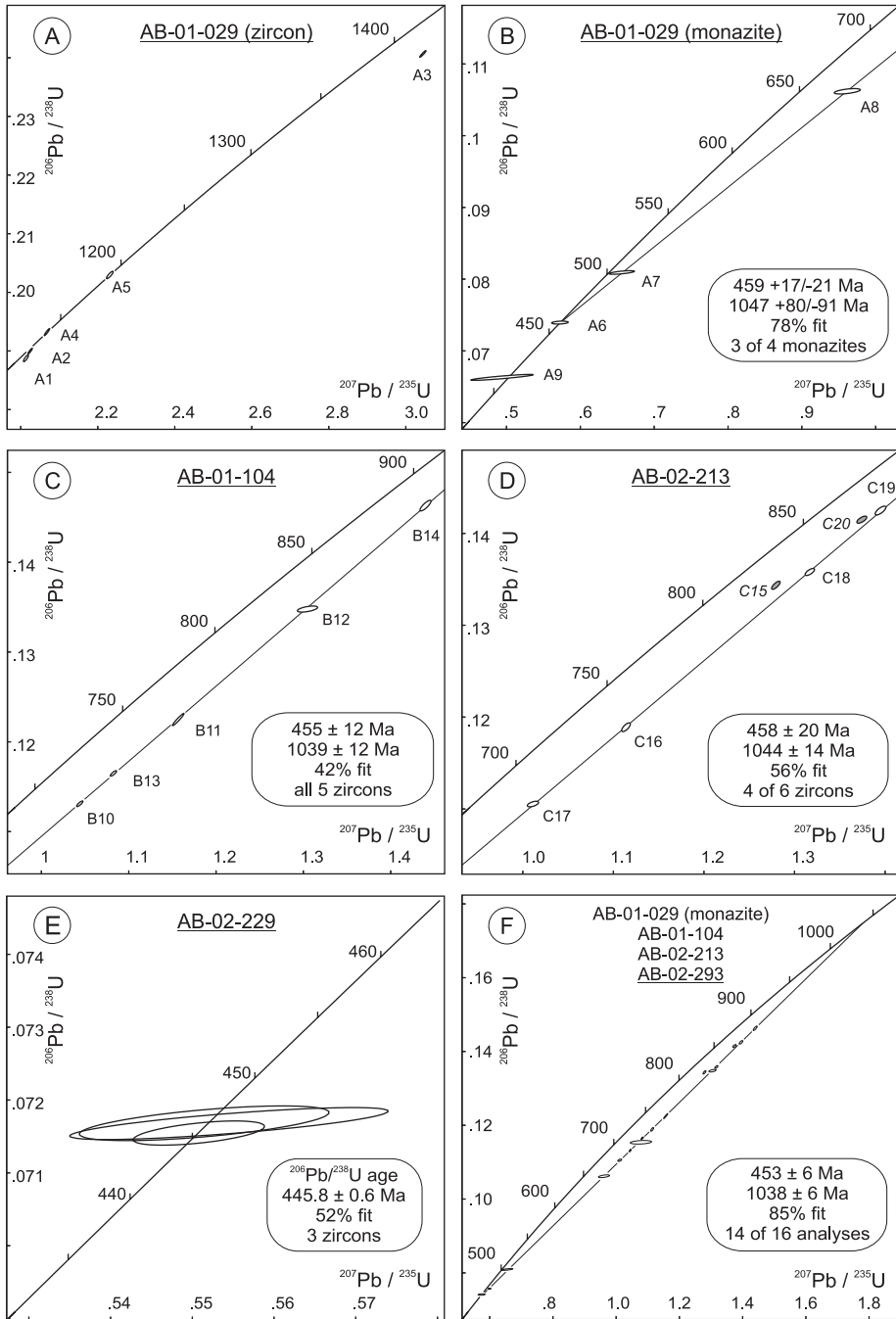Decay constants are from Jaffey and others (1971)

Fig. 6. U-Pb TIMS Concordia diagrams for samples from the BCZ (results in table 1): (A) Sample AB-01-029 (schistose muscovite granite) zircon grains; (B) Sample AB-01-029 (schistose muscovite granite) monazite grains; (C) Sample AB-01-104 (late syn-tectonic pegmatite dike); (D) Sample AB-02-213 (tectonized tonalite); (E) Sample AB-02-229 (foliated granodiorite sheet); and (F) compiled diagram including AB-01-029 monazite analyses, and AB-01-104, AB-02-213, and AB-02-293 ID-TIMS zircon analyses.

TABLE 2

U–Pb SHRIMP isotopic data for zircon from a mylonitic muscovite granite from the Little Grand Lake Fault, western Newfoundland

Spot name	U (ppm)	Th (ppm)	Th/U	Pb* (ppm)	^{204}Pb (ppb)	$\frac{^{204}Pb}{^{206}Pb}$	$\pm\frac{^{204}Pb}{^{206}Pb}$	$f(206)^{204}$	$\frac{^{208}Pb}{^{206}Pb}$	$\pm\frac{^{208}Pb}{^{206}Pb}$	$\frac{^{207}Pb}{^{235}U}$	$\pm\frac{^{207}Pb}{^{235}U}$	$\frac{^{206}Pb}{^{238}U}$	$\pm\frac{^{206}Pb}{^{238}U}$	Corr Coeff	$\frac{^{207}Pb}{^{206}Pb}$	$\pm\frac{^{207}Pb}{^{206}Pb}$	$\frac{^{206}Pb}{^{238}U}$	$\pm\frac{^{206}Pb}{^{238}U}$	$\frac{^{207}Pb}{^{206}Pb}$	$\pm\frac{^{207}Pb}{^{206}Pb}$
VB02-293 (Z7591): Mylonite muscovite granite, Little Grand Lake Fault (UTM 53784-4443)																					
7591-2.1	532	118	0.229	87	0	0.000002	0.000076	0.0000	0.0709	0.0038	1.7083	0.0460	0.1655	0.0022	0.588	0.0749	0.0016	987	12	1064	45
7591-7.1	542	29	0.056	37	3	0.000100	0.000242	0.0017	0.0158	0.0091	0.5594	0.0430	0.0748	0.0012	0.334	0.0543	0.0040	465	7	382	173
7591-24.1	1243	814	0.676	99	1	0.000010	0.000010	0.0002	0.2044	0.0080	0.5560	0.0139	0.0732	0.0011	0.703	0.0551	0.0010	455	7	417	40
7591-51.1	938	75	0.083	65	1	0.000010	0.000010	0.0002	0.0256	0.0018	0.5748	0.0130	0.0749	0.0009	0.648	0.0557	0.0010	466	6	439	39
7591-50.1	575	32	0.058	40	0	0.000010	0.000010	0.0002	0.0192	0.0022	0.5752	0.0148	0.0746	0.0010	0.629	0.0560	0.0011	464	6	451	45
7591-39.1	1034	66	0.066	71	2	0.000034	0.000093	0.0006	0.0194	0.0041	0.5579	0.0189	0.0747	0.0008	0.445	0.0542	0.0017	464	5	378	70
7591-48.1	1158	182	0.162	82	2	0.000024	0.000054	0.0004	0.0537	0.0033	0.5751	0.0225	0.0738	0.0014	0.570	0.0565	0.0018	459	8	472	73
7591-45.1	1425	144	0.105	100	1	0.000010	0.000010	0.0002	0.0336	0.0019	0.6023	0.0261	0.0746	0.0010	0.432	0.0586	0.0023	464	6	552	88
7591-24.2	763	309	0.418	57	13	0.000276	0.000142	0.0048	0.1258	0.0068	0.5399	0.0377	0.0738	0.0012	0.351	0.0531	0.0035	459	7	331	157

UTM measurements are in NAD-27 coordinates

Notes (see Stern, 1997):

Uncertainties reported at 1 sigma (absolute) and are calculated by numerical propagation of all known sources of error

$f206^{204}$ refers to mole fraction of total ^{206}Pb that is due to common Pb, calculated using the ^{204}Pb-method; common Pb composition used is the surface blank
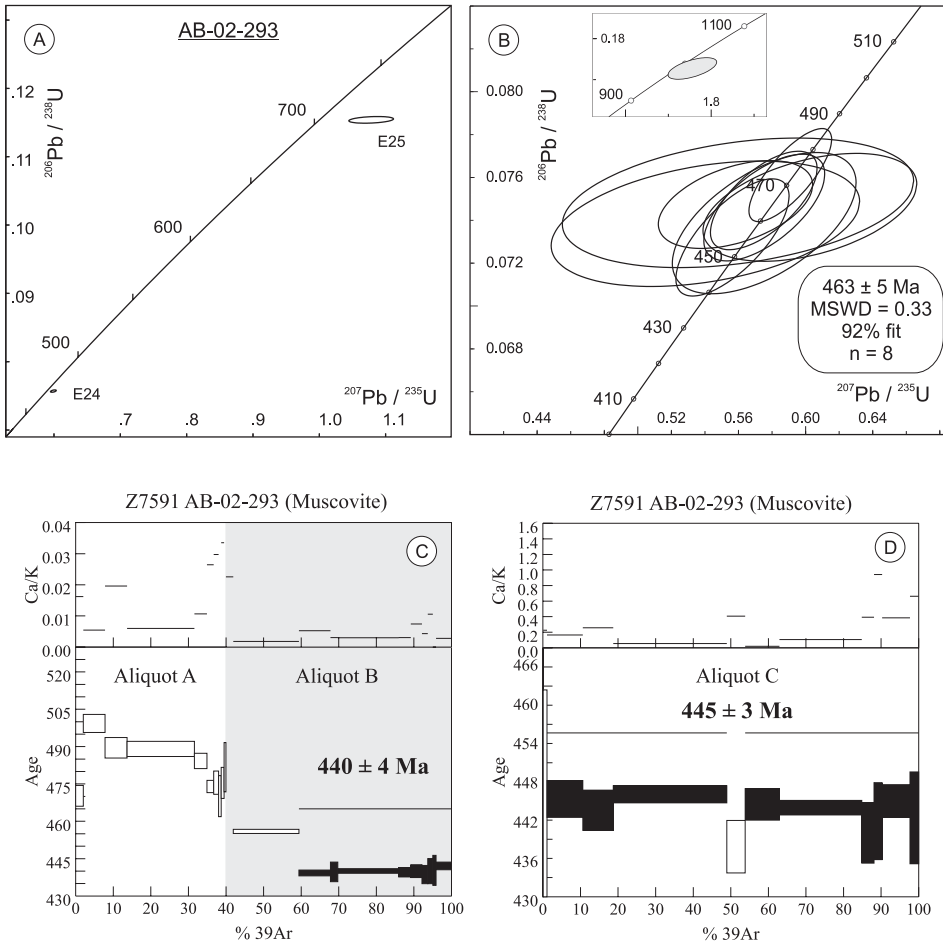
^{1204}-corrected ages (Stern, 1997)

Fig. 7. Results of various geochronological analyses on the mylonitic muscovite granite (sample AB-02-293) from the main strand of the Little Grand Lake Fault (results in tables 1 to 3): (A) U-Pb TIMS Concordia diagram of 2 zircon analyses; (B) U-Pb SHRIMP Concordia diagram of 8 analyses of tips of zircons. Inset shows one analysis yielding an older Grenvillian age, which was omitted from calculations; (C) and (D) ^{40}Ar/^{39}Ar muscovite geochronology age spectrum.

around their cores (fig. 8A). Since all analyzed grains had been abraded, such minor overgrowth could easily have been removed during the abrasion process, thereby exposing the cores. Therefore, the U-Pb zircon ages are most likely to represent ages of xenocrysts.

A few good-quality monazite grains were obtained from the sample. These grains are subhedral, clear to yellowish, and some grains have an orange (iron oxide?) coating on their surfaces. Four single monazite grains yielded data that are highly discordant (10.7 and 19.2%; grains A7 and A8), slightly discordant (-0.4% ; grain A6), as well as negatively discordant (-11.5% ; grain A9). Their ^{207}Pb/^{206}Pb ages range between 396 Ma and 808 Ma (table 1). The three older ^{207}Pb/^{206}Pb ages (grains A6 to A8) define a mixing line with a lower intercept at 459 $^{+17}/_{-21}$ Ma and an upper intercept at 1047 $^{+80}/_{-91}$ Ma (78% probability of fit; fig. 6B). The large error on the lower intercept is due to the large ^{207}Pb/^{235}U age error, but this lower intercept age is assumed to be fairly accurate, given the near-concordant position (-0.4%) and small

$^{40}Ar/^{39}Ar$ isotopic data from analyses on muscovite from a mylonitic muscovite granite from the Little Grand Lake Fault, western Newfoundland

Power[a]	Volume ^{39}Ar x10^{-11} cc	$^{36}Ar/^{39}Ar$	$^{37}Ar/^{39}Ar$	$^{38}Ar/^{39}Ar$	$^{40}Ar/^{39}Ar$	%^{40}Ar ATM	*$^{40}Ar/^{39}Ar$	f$_{39}$[b] (%)	Apparent Age Ma[c]
AB-02-293 Muscovite; J=.02344580[d] (Z7591; UTM 53784-4443)									
Aliquot:A									
2.4	7.1375	0.0016±0.0004	0.008±0.002	0.007±0.011	13.170±0.106	3.6	12.701±0.128	2.0	470.22±4.16
2.8	20.6033	0.0000±0.0001	0.003±0.001	0.004±0.011	13.606±0.109	0.0	13.600±0.113	5.8	499.30±3.62
3.0	20.8554	0.0001±0.0001	0.010±0.000	0.003±0.011	13.311±0.124	0.1	13.297±0.128	5.9	489.54±4.13
3.5	63.5564	0.0001±0.0001	0.003±0.000	0.003±0.011	13.303±0.094	0.2	13.281±0.094	17.9	489.05±3.04
3.9	11.9294	0.0001±0.0003	0.006±0.001	0.004±0.011	13.150±0.059	0.1	13.133±0.095	3.4	484.24±3.08
4.2	6.3127	0.0000±0.0002	0.014±0.002	0.003±0.011	12.821±0.053	0.0	12.817±0.075	1.8	474.00±2.45
4.6	4.6029	0.0001±0.0005	0.015±0.004	0.003±0.011	12.885±0.108	0.2	12.864±0.144	1.3	475.53±4.68
5.0	2.5498	0.0001±0.0012	0.028±0.003	0.004±0.011	12.742±0.130	0.4	12.697±0.253	0.7	470.12±8.25
6.0	2.7419	0.0004±0.0010	0.017±0.004	0.003±0.011	12.952±0.095	0.7	12.861±0.192	0.8	475.44±6.23
12.0	1.6448	0.0008±0.0016	0.029±0.003	0.004±0.011	13.240±0.148	1.4	13.055±0.306	0.5	481.73±9.92
Aliquot:B									
2.4	7.0515	0.0024±0.0004	0.012±0.001	0.006±0.011	11.644±0.046	6.1	10.930±0.101	2.0	411.57±3.39
2.8	62.0923	0.0001±0.0001	0.001±0.000	0.002±0.011	12.280±0.022	0.1	12.264±0.025	17.5	455.94±0.82
3.0	29.7775	0.0000±0.0001	0.003±0.000	0.003±0.011	11.759±0.031	0.0	11.758±0.036	8.4	439.24±1.18
3.3	7.0029	0.0002±0.0004	0.002±0.001	0.004±0.011	11.808±0.091	0.3	11.772±0.119	2.0	439.69±3.95
3.5	57.5608	0.0001±0.0000	0.002±0.000	0.002±0.011	11.797±0.026	0.1	11.782±0.028	16.2	440.04±0.92
3.7	11.3199	0.0000±0.0002	0.002±0.001	0.004±0.011	11.771±0.043	0.0	11.766±0.055	3.2	439.49±1.84
3.9	10.6197	0.0001±0.0003	0.004±0.001	0.005±0.011	11.793±0.057	0.1	11.781±0.077	3.0	439.99±2.56
4.2	5.5519	0.0001±0.0005	0.002±0.002	0.003±0.011	11.763±0.050	0.2	11.739±0.110	1.6	438.62±3.65
4.6	4.6737	0.0001±0.0005	0.005±0.002	0.006±0.011	11.799±0.102	0.2	11.780±0.153	1.3	439.98±5.06
5.5	3.0601	0.0001±0.0006	0.000±0.000	0.006±0.011	11.816±0.088	0.2	11.789±0.181	0.9	440.28±6.01
12.0	14.6262	0.0000±0.0001	0.001±0.001	0.002±0.011	11.848±0.033	0.0	11.844±0.047	4.1	442.08±1.56
AB-02-293 Muscovite; J=.02925380[d] (Z7591; UTM 53784-4443)									
Aliquot: C									
2.0	0.0561	0.0501±0.0117	20.549±9.051	0.074±0.023	15.967±1.743	51.4	7.754±4.658	0.1	368.84±200.53
2.4	0.7537	0.0097±0.0019	0.118±0.636	0.015±0.011	11.589±0.149	19.2	9.364±0.599	1.0	436.77±24.81
2.8	7.1533	0.0010±0.0002	0.085±0.057	0.002±0.011	9.758±0.041	2.0	9.561±0.068	9.5	444.92±2.82
3.0	6.0956	0.0004±0.0002	0.134±0.072	0.002±0.011	9.554±0.052	0.4	9.519±0.074	8.1	443.20±3.07
3.5	22.6758	0.0002±0.0000	0.029±0.015	0.002±0.011	9.625±0.031	0.5	9.578±0.032	30.2	445.63±1.31
3.9	3.6759	0.0003±0.0002	0.211±0.110	0.003±0.011	9.386±0.060	0.0	9.385±0.097	4.9	437.64±4.00
4.2	6.8516	0.0004±0.0002	0.010±0.062	0.001±0.011	9.573±0.034	0.3	9.541±0.058	9.1	444.09±2.41
4.6	16.4352	0.0001±0.0000	0.055±0.024	0.002±0.011	9.526±0.022	0.0	9.529±0.027	21.9	443.60±1.12
5.0	2.4616	0.0008±0.0003	0.205±0.161	0.002±0.011	9.472±0.058	0.4	9.435±0.111	3.3	439.73±4.61
5.5	1.6092	0.0005±0.0005	0.490±0.317	0.002±0.011	9.490±0.102	0.1	9.479±0.142	2.1	441.54±5.87
6.5	5.5769	0.0004±0.0001	0.200±0.103	0.003±0.011	9.574±0.038	0.2	9.553±0.060	7.4	444.61±2.50
12.0	1.7199	0.0007±0.0004	0.345±0.222	0.002±0.011	9.501±0.096	0.1	9.491±0.170	2.3	442.04±7.02

a: As measured by laser in % of full nominal power (10W)
b: Fraction ^{39}Ar as percent of total run
c: Errors are analytical only and do not reflect error in irradiation parameter J
d: Nominal J, referenced to PP-20=1072 Ma (Roddick, 1983)
All uncertainties quoted at 2σ level; UTM measurements are in NAD-27 coordinates

error on the $^{206}Pb/^{238}U$ age of grain A6. Back-scattered SEM-imaging shows that most of the monazite grains are heterogeneous, having a complex core and a featureless gray rim (figs. 8B and 8C).

The schistose granite shows a complex U-Pb history and different explanations for the U-Pb ages are possible. Based on regional correlation, our preferred hypothesis is
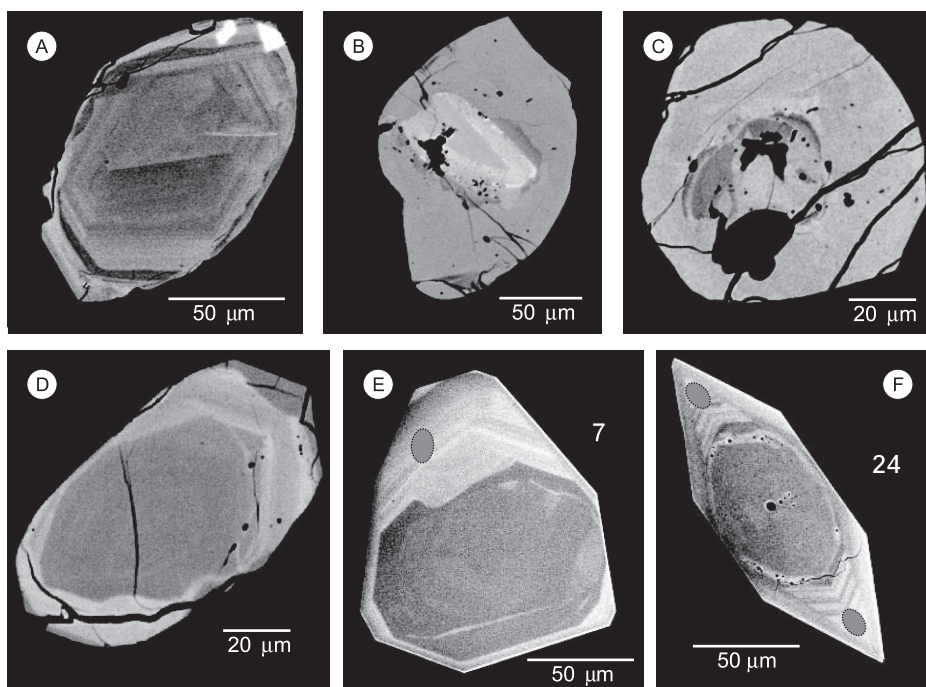
Fig. 8. Back-scattered electron images of zircon and monazite from U-Pb geochronological samples. (A) Sample AB-01-029 (schistose muscovite granite), zircon grain showing an oscillatory zoned core with a narrow overgrowth; (B) Sample AB-01-029 (schistose muscovite granite), monazite grain showing wide featureless rim around a complex zoned core; (C) Sample AB-01-029 (schistose muscovite granite), monazite grain showing wide featureless rim around a heterogeneous resorbed (?) core. The large ovoid dark area towards the bottom is a zircon inclusion; the triangular black areas in the core are inclusions of xenotime and feldspar; (D) AB-02-213 (tectonized tonalite), zircon grain showing evidence for resorption (lower part of grain), and euhedral overgrowth (top of grain); (E and F) AB-02-293 (mylonitic muscovite granite), zircon grains with euhedral overgrowth with oscillatory magmatic zoning. The gray ellipses mark the location of SHRIMP spot; the numbers refer to the grain analyzed (see table 2).

that the lower intercept of *circa* 459 Ma represents the age of emplacement of the granite. The upper intercept of *circa* 1047 Ma would indicate that the average age of the inherited monazite grains is Grenvillian. Also, all zircon ages can be interpreted as Mesoproterozoic inheritance and the minor overgrowths are most likely Ordovician in age and magmatic in origin. An alternative interpretation is that the concordant zircon grains around 1130 Ma (grains A1, A2 and A4) represent the age of emplacement of the granite. The monazite discordia line would represent two distinct metamorphic events: a subsequent Grenvillian and an Ordovician event. In this scenario, the zircon overgrowths can be interpreted as being metamorphic or hydrothermal.

There is no irrefutable evidence to support either interpretation, but the important conclusion that can be drawn from the complex U-Pb ages of this schistose granite is that it has recorded at least one Grenvillian and an Ordovician dynamo-thermal event. The interpretation of this granite is even more complicated by the fact that a fourth monazite grain (grain A9; table 1) is concordant within error but gives a younger $^{206}Pb/^{238}U$ age of 414 ± 3 Ma. This may reflect lead-loss or monazite growth related to movement in the BCZ after emplacement of the granite.

Late syn-tectonic pegmatite dike (AB-01-104).—A sample was taken from the folded, late syn-tectonic pegmatite dike described above (fig. 5A), in order to constrain the age of medium- to high-grade deformation in the BCZ (fig. 2B). The sample yielded a

small number of zircon grains, which predominantly have a stubby morphology. The grains are colorless to slightly brownish and have few inclusions. All five analyzed zircon grains define a best-fit regression line (42% probability of fit; fig. 6C) with a lower intercept of 455 ± 12 Ma and an upper intercept of 1039 ± 12 Ma. The lower intercept is interpreted as the age of intrusion of the pegmatite. Moreover, it constrains the minimum age of the main phase of high-grade deformation along the BCZ to be Middle to Late Ordovician (Taconic). Unfortunately, the error on the lower intercept is rather large, because the analyses have limited spread and plot near the middle of the discordia line. The upper intercept shows that the inherited grains in the pegmatite are Mesoproterozoic (Grenvillian) in age.

Tectonized tonalite (AB-02-213).—In the southwestern part of our study area, a tonalite with a strong gneissic fabric is exposed (fig. 2B). The tonalite contains mafic and ultramafic xenoliths of variable size and shape, some of which contain a pre-incorporation fabric. The strong tectonic fabric in the tonalite suggests that significant deformation occurred after emplacement of the tonalite. A sample was taken from a relatively homogenous and xenolith-free section of the outcrop.

The sample contains abundant zircons, which were divided into two populations: a euhedral elongate and a multifaceted ovoid population. Zircon grains of the former population are of simple morphology, variable size, elongate, and clear. Most grains contain small melt inclusions, which, when present, are located in the central part of the grains. Some grains have visible cores and associated overgrowths. Back-scattered SEM-imaging of a random population of zircon from the sample shows that most grains have clear subdomains of cores and overgrowths. The cores are characterized by oscillatory zoning and the wide rims, which generally have euhedral crystal faces, occasionally show a faint zoning pattern. Some boundaries between the cores and overgrowths are very irregular, which is indicative of resorption (fig. 8D). Based on the morphology of most zircon grains from both populations, heterogeneity within the grains was expected. Three single zircon grains were analyzed: two from the elongate population (grains C15 and C16), and one from the multi-facetted population (grain C17; table 1). In addition, one zircon fragment (grain C20) was analyzed, and two analyses were done on tips of grains (grains C18 and C19), which were carefully detached from their respective cores. When constructing a mixing line using all six analyses, the analyses lie scattered, half way between the lower and upper intercept of a discordia line (443 ± 20 and 1017 ± 11 Ma intercepts), but probability of fit is very low. Analyses of the two tips and the fragment actually yielded the oldest ^{207}Pb/^{206}Pb ages (table 1). A best-fit regression line that fits four of the data within error (grains C16 to C19) yields an upper intercept of 1044 ± 14 Ma and a lower intercept of 458 ± 20 Ma (56% probability of fit; fig. 6D). The large errors on both intercepts prevent a precise interpretation of the age of emplacement of the tonalite, but the data show that the tonalite was emplaced in the Middle to Late Ordovician. The upper intercept shows that there is an important xenocrystic Grenvillian component that is very similar to the previously discussed samples (*circa* 1.04 Ga).

Foliated granodiorite sheet (AB-02-229).—A sample was taken from a foliated granodiorite sheet that is interlayered on a meter- to decameter-scale with strongly deformed mélange metasediments (figs. 2B and 4B). The coarser-grained and xenolith-free granodiorite has a weak foliation, in contrast with the strongly deformed and heterogeneous paragneiss, which may indicate that the granodiorite intruded syn- or inter-tectonically. Associated sheath folds (fig. 4A) and winged objects (fig. 4B) indicate oblique-dextral deformation. Locally, the granodiorite is observed to have commingled with a more mafic magma (diorite).

Two populations of zircon grains were identified in the sample: a population of ovoid, multi-facetted zircons, and a population of large elongate, needle-like zircon

grains. The elongate zircon grains are clear, contain some melt inclusions, and are of simple morphology. The grains of the multi-facetted population are of various sizes, stubby in shape, inclusions are absent, and some grains show visible overgrowth. Based on morphology, grains of the former population are interpreted as having formed in the parent magma, whereas the grains of the multi-facetted population would most likely contain inherited cores with younger overgrowth (similar to samples AB-02-213 and AB-02-293). Three zircon grains were analyzed, two of the elongate morphology (grains D21 and D22; table 1), and one of the multi-facetted population (grain D23; table 1). The analyses yielded concordant data with $^{206}Pb/^{238}U$ ages within error. The 2σ-error on the $^{207}Pb/^{235}U$ ages is large, in contrast with the $^{206}Pb/^{238}U$ ages. Therefore, the average age of 445.8 ± 0.6 Ma (52% probability of fit; fig. 6E) for the foliated granodiorite is based on the $^{206}Pb/^{238}U$ age and is interpreted to be the age of emplacement of the granodiorite.

Mylonitic muscovite granite, Little Grand Lake Fault (AB-02-293).—In order to obtain the age of deformation on the LGLF, a sample from the main strand of the LGLF at the southeastern end of Little Grand Lake was collected (fig. 2A). The protolith in which the shear zone has developed, is a plagioclase-rich muscovite granite that was emplaced into a metasedimentary unit. The sample has a strong mylonitic fabric. Both U-Pb (ID-TIMS and SHRIMP) and $^{40}Ar/^{39}Ar$ analyses were performed (fig. 7).

U-Pb Geochronology: The sample yielded abundant zircons, most of which are multifaceted and euhedral. Zircon grains are clear, stubby, sometimes distinctly bipyramidal, and some grains contain opaque and melt inclusions. Overgrowths, especially on the larger grains, are commonly visible under a binocular microscope.

Initial U-Pb TIMS analyses of two zircon grains (table 1) gave discordant (9 and 19%) results with different $^{207}Pb/^{206}Pb$ ages (fig. 7A). A mixing line based on these analyses has a Late Ordovician lower intercept and a Mesoproterozoic upper intercept, indicative of heterogeneity within the zircon grains. Cores are overgrown by bright rims that are characterized by magmatic oscillatory zoning, which are clearly apparent in back-scattered SEM-images (figs. 8E and 8F). Consequently, *in-situ* analyses of the overgrowths were undertaken on SHRIMP. Eight of the analyses were pooled and a Concordia age of 463 ± 5 Ma (92% probability of fit; MSWD = 0.33; fig. 7B) was calculated. One SHRIMP analysis yielded a discordant Mesoproterozoic age (1064 Ma $^{207}Pb/^{206}Pb$ age; table 2; fig. 7B inset), which is interpreted as an inherited age based on the abundance of heterogeneous grains in this sample. The age (*circa* 1.0 Ga) is again similar to the age of inheritance of other samples in this study. All fractions have high uranium content (532 – 1425 ppm) and Th/U ratios vary between 0.06 and 0.68 (table 2). The date of 463 ± 5 Ma is interpreted as the age of emplacement of the muscovite granite protolith.

$^{40}Ar/^{39}Ar$ *Geochronology:* Two separate analyses on muscovite separates from the mylonitic muscovite granite sample were completed. The first analysis was comprised of two aliquots (table 3, fig. 7C). The first aliquot analyzed has quite a bit of scatter (aliquot A; table 3) and all of the steps are radiogenic. The scatter most likely indicates the presence of some sort of contaminant degassing, perhaps K-feldspar inclusions in the muscovite. The second aliquot (aliquot B; table 3) reveals the presence of excess Ar in the first 2 steps; however, it yields a well-defined plateau, comprising 68 percent of the total gas and defining the age of the aliquot to be 440 ± 4 Ma (table 3, fig. 7C). As the two aliquots from the first analysis were not in agreement, further analysis of muscovite from this sample was undertaken. A second analysis of muscovite yielded a well-defined plateau age, comprising 95 percent of total gas emitted (table 3, fig. 7D) and defining the age of the sample at 445 ± 3 Ma. These $^{40}Ar/^{39}Ar$ cooling ages (aliquots B and C) are within error.

The temperature condition under which the mylonitic fabric has formed (see discussion above) was above or near the muscovite closure temperature for argon (*circa* 350°C; McDougall and Harrison, 1999). Therefore the muscovite ages represent either the age at which this mylonitic rock cooled below 350°C, or the actual crystallization age of muscovite and hence the age of deformation on the LGLF. Thus, south-side-up deformation on the LGLF is constrained to have occurred between late Middle Ordovician and the earliest Silurian, between 463 ± 5 Ma and 440 ± 4 Ma. However, considering that most of the motion on the LGLF took place after peak metamorphism in the Dashwoods block (see above), which lasted no later than circa 456 Ma (van Staal and others, 2007) we interpret the muscovite to have predominantly grown during retrograde conditions. Hence, the motion along the LGLF mainly took place during the latest Ordovician to earliest Silurian (450 – 440 Ma).

INTERPRETATION AND DISCUSSION

Ordovician Plutonism in the Dashwoods Subzone

Except for the foliated granodiorite sheet (AB-02-229), all samples yielded late Mesoproterozoic upper intercepts (*circa* 1.04 Ga) as well as Ordovician lower intercepts (*circa* 0.45 Ga), but unfortunately each sample has a relatively large error on both intercepts. When combining the analyses of these four samples (AB-01-029, AB-01-104, AB-02-213, and ID-TIMS analyses of AB-02-293), a mixing line can be constructed based on 3 monazite (grains A6 to A8) and 11 zircon data (grains B10 to B14, C16 to C19, and E24 and E25; table 1; fig. 6F), yielding an upper intercept of 1038 ± 6 Ma, and a lower intercept of 453 ± 6 Ma (85% probability of fit).

This diagram demonstrates the regional importance of the late Middle to Late Ordovician magmatic event – the voluminous second phase of the Notre Dame Arc (van Staal, 2007) – that has affected the Dashwoods subzone. This magmatic event is coeval with regional deformation in the Dashwoods subzone and has been interpreted to represent the collision of Dashwoods with the Laurentian margin (van Staal and others, 2007). Additionally, the diagram demonstrates the regional development of a source of Grenvillian affinity to the Dashwoods subzone, which is important for paleogeographical reconstructions (see discussion below). Last of all, the diagram also demonstrates that, based on its U-Pb ages, the schistose muscovite granite (AB-01-029) exposed in the cataclastic zone of the BCZ has a closer relationship with Dashwoods subzone units than with the Neoproterozoic Hare Hill Complex of the internal Humber Zone (Currie and van Berkel, 1992), and therefore the schistose granite is assigned to the Dashwoods subzone.

Oblique-Dextral Deformation Along the BCZ

In Late Ordovician time (*circa* 455 Ma) the western boundary of the Dashwoods subzone experienced oblique-dextral deformation under medium- to high-grade conditions, as exemplified by the syn-tectonic pegmatite dike (AB-01-104). Similar observations have been made along the Humber Zone - Dunnage Zone boundary throughout the northern Appalachians. In the Three Pond area of the Dashwoods subzone (15 km northeast of fig. 2B), a belt of anastomosing shear zones, which are spatially related to (ultra) mafic lenses in the metasediments, is exposed. These N-S striking high-strain zones have a predominant dextral sense of shear, were demonstrated to post-date peak regional metamorphism and migmatization (*circa* 460 Ma; Piasecki, 1988), and were inferred to be pre-Silurian (Piasecki, 1995). In the Baie Verte peninsula in northern Newfoundland, the Baie Verte Brompton Line (BBL in fig. 1) has registered a complex deformation history that includes ductile transcurrent (both dextral and sinistral), and dip-slip movements (Hibbard, 1983; Goodwin and Williams, 1990; Piasecki, 1995). No direct geochronological ages have been associated with these

deformational phases, but it was postulated that two ductile dextral strike-slip motions have occurred, the younger of which is associated with greenschist facies deformation and is younger than Early Silurian (Goodwin and Williams, 1996). The older dextral movement in the Baie Verte Brompton Line is most likely Middle to Late Ordovician and related to the Taconic orogeny (conform Williams and St-Julien, 1982). To the south in the Québec Appalachians, the Shickshock Sud fault zone, a fault system spatially associated with the BCZ, has also been shown to accommodate oblique-dextral movement during the Late Ordovician (454 – 456 Ma; Sacks and others, 2004). Thus late Middle to Late Ordovician (oblique-) dextral deformation along the Laurentian (Humber) margin has been recognized throughout the northern Appalachians.

The 445.8 ± 0.6 Ma latest Ordovician granodiorite sheet (AB-02-229) in the western Dashwoods subzone is similar in age and composition to the *circa* 449 Ma Pin pluton (Hall and van Staal, 1999) in the southern Dashwoods subzone, and the *circa* 440 Ma Glover Island and Burlington granodiorite bodies in the northern Notre Dame subzone (Cawood and van Gool, 1998). This geographically widespread group of granitoid bodies represents the third phase of the Notre Dame Arc (see fig. 2 in van Staal, 2007), which is interpreted to post-date the Taconic orogeny (*sensu* van Staal and others, 2007). The granodiorite sheet has also been affected by oblique-dextral deformation, and therefore the Late Ordovician deformation in the BCZ continued (possibly intermittently) into the Early Silurian with a similar sense of shear along its boundary. This also implies that oblique-dextral deformation along the western boundary of Dashwoods under medium- to high-grade conditions is not restricted to the Taconic orogeny, but continued after the main collision of Dashwoods with the Laurentian margin. Post-collisional movements along the boundaries of individual tectonic segments, especially lateral movements along crustal-scale boundaries such as the BCZ, are to be expected in a southwest Pacific Ocean type tectonic setting (van Staal and others, 1998).

Regional Tectonic Setting and the LGLF

The late Middle to Late Ordovician oblique-dextral movement along the western boundary of Dashwoods is contemporaneous with oblique-sinistral accretion of the Annieopsquatch Accretionary Tract along its eastern margin (Lissenberg and others, 2005; Zagorevski and others, 2006). However, it is unlikely that these motions were coupled dynamically, since both of them are related to different convergence systems (Waldron and van Staal, 2001; Zagorevski and others, 2006). This implies that during the late Middle to Late Ordovician, the Dashwoods microcontinent moved in a southerly direction with respect to Laurentia to the west and the then-present Iapetus Ocean to the east (fig. 9).

Deformation on the LGLF is probably late Ordovician to earliest Silurian in age (450 – 440 Ma) suggesting that the dextral-reverse movement along the LGLF is contemporaneous with the Late Ordovician deformation in the BCZ. If the oceanic Snooks Arm arc and the continental Notre Dame Arc formed part of the same continuous arc system, comparable to the present-day Banda and Sunda arc system in Indonesia (van Staal, 2007), the Snooks Arm arc and its Baie Verte Oceanic Tract infrastructure may have moved independently and faster southwards than the Notre Dame Arc with its Dashwoods substrate. Such convergence would have made the LGLF a contractional bend in an overall arc-parallel strike-slip fault system (fig. 9). Hence a faster moving Snooks Arm arc could have underthrusted the Dashwoods microcontinent with its Notre Dame Arc suprastructure, juxtaposing the higher-grade rocks of the latter with lower grade volcanic rocks of the Snooks Arm arc.

Inherited Grains and Dashwoods Microcontinent Correlatives

The presence of Late Mesoproterozoic (1030 – 1190 Ma; fig. 6) inheritance in several igneous rock units of the Dashwoods subzone (tables 1 and 2) has tectonic implications with respect to paleogeographic reconstructions. The fact that a well-defined mixing line can be constructed using the analyses of four different samples (fig. 6F) demonstrates the regional presence of a crustal source with a Grenville affinity in the Dashwoods subzone. It is unclear whether the inherited grains from our samples were derived from the crystalline basement to the Dashwoods subzone or its overlying sediments.

In addition to previously recognized Early Mesoproterozoic (1300 – 1650 Ma) inherited ages (for example, Dunning and others, 1989; Whalen and others, 1997), the presence of Grenvillian inherited ages in the Dashwoods subzone strengthens the argument for relating Dashwoods to the Long Range Inlier of northern Newfoundland, where crystalline units of similar ages (1.5 and 1.0 Ga) are exposed (fig. 1; Heaman and others, 2002). To the west, the Long Range Inlier is tectonically emplaced onto 'its' Cambro-Ordovician passive margin sequence, but along its northern and southern margin the rift-drift clastics and subsequent passive margin carbonates are unconformably overlying the Long Range Inlier (Williams, 1995). Therefore, the Long Range Inlier cannot represent the Dashwoods microcontinent *sensu stricto*, but the two crystalline segments appear to have a similar Mesoproterozoic history and hence may have been adjacent to one another prior to rifting, opening of the Humber seaway and departure of Dashwoods.

Our new ages also introduce a possible connection of the Dashwoods subzone with the Blair River Inlier in Cape Breton Island, Nova Scotia. This crystalline complex is composed of various plutonic rocks of Grenvillian age (978 – 1080 Ma), and even though no ages older than 1.2 Ga have been identified, Sm-Nd depleted mantle model
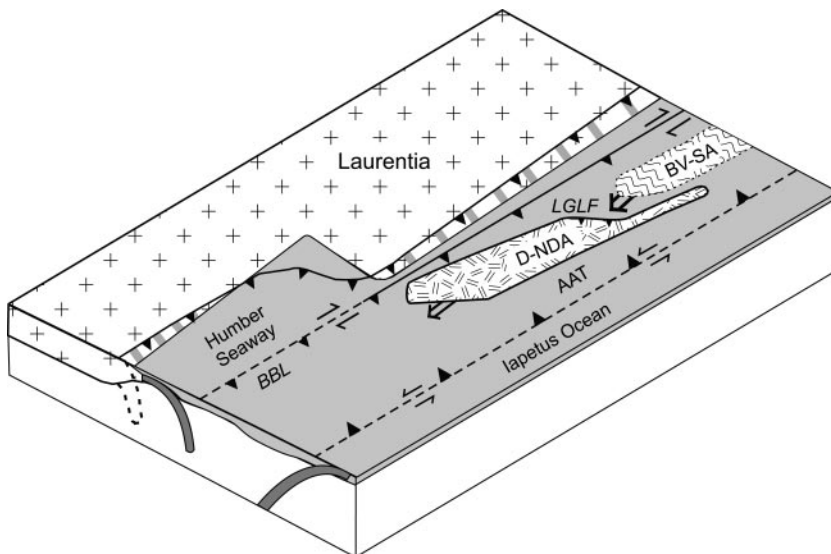

Fig. 9. A tectonic model for the Dashwoods microcontinent and associated Notre Dame Arc during the Middle to Late Ordovician. The model shows the southward translation of Dashwoods microcontinent and its associated Notre Dame Arc (D-NDA), with respect to the Laurentian margin and the Annieopsquatch Accretionary Tract (AAT). It also shows the interaction along the Little Grand Lake Fault (LGLF) between the Baie Verte Oceanic Tract with its Snooks Arm arc (BV-SA) and the Dashwoods microcontinent (modified from van Staal, 2007).

ages from gneisses in the area suggest the presence of an older Mesoproterozoic component of *circa* 1.5 Ga (Dickin and Raeside, 1990; Miller and others, 1996). The Blair River Inlier is generally interpreted, but not definitely confirmed, to be Humber Zone basement. Its isolated position, the absence of overlying Cambro-Ordovician sediments, and its tectonic contact with peri-Gondwanan units allow for different interpretations of its provenance (Miller and others, 1996; and references therein). Could it be possible that the Blair River Inlier formed part of the Dashwoods microcontinent? Both segments have been affected by Silurian (435 – 425 Ma) magmatism. However, the Ordovician tectono-magmatic event characteristic of the Dashwoods subzone has not been identified in the Blair River Complex. If the Blair River Inlier indeed formed part of the Dashwoods microcontinent, it is important to explain the absence of this Ordovician tectono-magmatic event. The Blair River Inlier could have been 1) along-strike with the Notre Dame Arc, in a tectonic setting where the subducting crust was situated too shallow or too deep below the overlying crust to allow for arc magmatism to occur (Cross and Pilger, 1982); or 2) in front of the Notre Dame Arc (forearc region). In both locations, these segments would not have been affected by Ordovician magmatism. The absence of an Ordovician dynamo-thermal event could have been attained when, for example, the Blair River Inlier was situated either in or in front of a re-entrant, and Dashwoods was opposed to a promontory. In this scenario, the Blair River Inlier would have escaped the (hard) collision that affected the Dashwoods.

Based on the evidence, it is possible that the Blair River Inlier and/or the Long Range Inlier represents Dashwoods basement. However, important queries, including the marked discrepancy in Nd isotopic values between the Dashwoods and the two basement inliers (Whalen and others, 1997), have to be addressed in order to allow for a positive correlation.

<div align="center">CONCLUSIONS</div>

Our conclusions can be summarized as follows:
1. The western boundary of the Dashwoods microcontinent experienced oblique-dextral deformation from Late Ordovician into Early Silurian either continuously or intermittently, based on the presence of a late syn-tectonic pegmatite dike (455 ± 12 Ma) and a foliated granodiorite sheet (446 ± 1 Ma). Deformation along the Humber Zone – Dunnage Zone boundary, which has been observed throughout the northern Appalachians, is contemporaneous with oblique-sinistral accretion of peri-Laurentian units (Annieopsquatch Accretionary Tract) to the eastern margin of the Dashwoods microcontinent. This suggests that the Dashwoods microcontinent had a southward translation during the Middle to Late Ordovician (fig. 9).
2. U-Pb and $^{40}Ar/^{39}Ar$ geochronology combined with other geological evidence confirms that Late Ordovician-earliest Silurian (ca. 450 – 440 Ma) dextral-reverse movement along the Little Grand Lake Fault (LGLF), which juxtaposed low-grade oceanic units to the north with medium- to high-grade metasedimentary units to the south, is coeval with the southward translation of the Dashwoods microcontinent.
3. New U-Pb geochronology data, including a muscovite granite (463 ± 5 Ma), a schistose muscovite granite (459 $^{+17}/_{-21}$ Ma), and a tectonized tonalite (458 ± 20 Ma), demonstrate the regional importance in the Dashwoods subzone of the voluminous Middle Ordovician magmatic pulse (second phase of the Notre Dame Arc).
4. The presence of numerous *circa* 1.04 Ga old (Grenvillian *sensu stricto*) inherited grains in several igneous units is important for paleogeographical reconstruction of the Dashwoods microcontinent. It reinforces the link of the Dashwoods

basement with the Long Range Inlier in western Newfoundland. Moreover, it introduces a possible link with the Blair River Inlier in Cape Breton. Based on U-Pb ages, it is feasible that this segment formed part of the Dashwoods microcontinent during the Ordovician.

APPENDIX

ANALYTICAL TECHNIQUES

U-Pb ID-TIMS

Single grain zircon and monazite U-Pb ID-TIMS analyses were performed at the Jack Satterly Laboratory, University of Toronto and at the Royal Ontario Museum. Mineral concentrates were prepared using standard methods involving crushing, grinding, a Wilfley[TM] table, heavy liquids, and the Frantz[TM] isodynamic separator successively. Grains were examined and handpicked using a binocular microscope. Standard methods of bomb dissolution (for zircon) and U-Pb extraction with HCl in small anion exchange columns were used (Krogh, 1973, 1982), although several small zircon grains were analyzed without chemical purification (marked ** in table 1). Selected monazite grains were dissolved in 6N HCl in Savillex[TM] capsules, and processed with HCl in small anion exchange columns. Pb and U were loaded together with silica gel onto out-gassed rhenium filaments. The isotopic compositions of Pb and U were measured using a single collector Daly detector in a solid source VG354 mass spectrometer. Data were calculated, regressed and plotted using the UTILAge software (D.W. Davis, in-house program) with regression based on Davis (1982). All age errors quoted in the text and table 1, and error ellipses in the Concordia diagrams, (figs. 6 and 7A) are given at the 95 percent confidence interval.

U-Pb SHRIMP

SHRIMP II analyses were conducted at the Geological Survey of Canada (GSC) using analytical procedures described by Stern (1997), with standards and U-Pb calibration methods following Stern and Amelin (2003). Handpicked zircon grains from sample AB-02-293 (z7591) were cast in 2.5 cm diameter epoxy mounts (GSC mount #304) along with fragments of the GSC laboratory standard zircon (z6266, with $^{206}Pb/^{238}U$ age = 559 Ma). The midsections of the zircon grains were exposed using 9, 6, and 1 μm diamond compound, and the internal features of the zircons were characterized with backscatter electrons (BSE) and cathodo-luminescence (CL) utilizing a Cambridge Instruments scanning electron microscope (SEM). Mount surfaces were evaporatively coated with 10 nm of high purity Au. Analyses were conducted using an $^{16}O^-$ primary beam, projected onto the zircon grains at 10 kV. The sputtered area used for analysis was *circa* 12 μm in diameter with a beam current of *circa* 1.3 nA. The count rates of ten isotopes of Zr^+, U^+, Th^+, and Pb^+ in zircon were sequentially measured over 5 scans with a single electron multiplier and a pulse counting system with deadtime of 35 ns. Off-line data processing was accomplished using customized in-house software. The 1σ external error of $^{206}Pb/^{238}U$ ratios reported in table 2 incorporate a ±1.0 percent error in calibrating the standard zircon (see Stern and Amelin, 2003). No fractionation correction was applied to the Pb-isotope data; common Pb correction utilized the measured $^{204}Pb/^{206}Pb$ and compositions modeled after

Cumming and Richards (1975). The $^{206}Pb/^{238}U$ ages for the analyses have been corrected for common Pb using both the 204- and 207-methods (Stern, 1997), but there is generally no significant difference in the results (table 2). Isoplot v. 2.49 (Ludwig, 2001) was used to generate a Concordia diagram where the data are plotted with errors at the 2σ-level (fig. 7B). The calculated Concordia age and errors quoted in the text are at 2σ with decay constant errors included (Ludwig, 1998).

$^{40}Ar/^{39}Ar$ Geochronology

Laser $^{40}Ar/^{39}Ar$ step-heating analysis was carried out at the Geological Survey of Canada laboratories in Ottawa, Ontario. Sample AB-02-293 was processed for $^{40}Ar/^{39}Ar$ analysis of muscovite phenocrysts by standard mineral separation techniques, including handpicking of clear, unaltered crystals in the size range 0.5 to 1 mm. Individual mineral separates were loaded into aluminum foil packets along with PP-20 hornblende (Hb3gr equivalent) with an apparent age of 1072 Ma (Roddick, 1983) to act as flux monitor. The sample packets were arranged radially inside an aluminum can. The samples were then irradiated for 70 (aliquots A and B) and 120 (aliquot C) hours at the research reactor of McMaster University in a fast neutron flux of approximately $3x10^{16}$ neutrons/cm^2.

Upon return from the reactor, samples were split into several aliquots and loaded into individual 1.5 mm-diameter holes in a copper planchet. The planchet was then placed in the extraction line and the system evacuated. Heating of individual sample aliquots in steps of increasing temperature was achieved using a Merchantek MIR10 10W CO_2 laser equipped with a 2 mm x 2 mm flat-field lens. The released Ar gas was cleaned over getters for ten minutes, and then analyzed isotopically using the secondary electron multiplier system of a VG3600 gas source mass spectrometer; details of data collection protocols can be found in Villeneuve and MacIntyre (1997) and Villeneuve and others (2000). Error analysis on individual steps follows numerical error analysis routines outlined in Scaillet (2000); error analysis on grouped data follows algebraic methods of Roddick (1988).

Corrected argon isotopic data are listed in table 3, and presented as spectra of gas release (figs. 7C and 7D; Roddick and others 1980). Figure 7C represents a gas-release spectrum that contains stepheating data from two aliquots, alternately shaded and normalized to the total volume of ^{39}Ar released. Such plots provide a visual image of replicated heating profiles and the error and apparent age of each step.

Neutron flux gradients throughout the sample canister were evaluated by analyzing the hornblende flux monitors included with each sample packet and interpolating a linear fit against calculated J-factor and sample position. The error on individual J-factor values is conservatively estimated at ±0.6 percent (2σ). Because the error associated with the J-factor is systematic and not related to individual analyses, correction for this uncertainty is not applied until calculation of dates from isotopic correlation diagrams (Roddick, 1988). All errors are quoted at the 2σ level of uncertainty.

References

Bédard, J. H., Lauzière, K., Tremblay, A., Sangster, A., Douma, S. L., and Dec, T., 2000, Betts Cove Ophiolite and its cover rocks, Newfoundland: Geological Survey of Canada Bulletin, 550, 76 p.

Brem, A. G., ms, 2007, The Late Neoproterozoic to Early Palaeozoic tectonic evolution of the Long Range Mountain, southwestern Newfoundland: Waterloo, Canada, University of Waterloo, Ph. D. Thesis, 166 p.

Brem, A. G., Lin, S., and van Staal, C. R., 2002, Humber Zone - Dunnage Zone relationships and the Long Range Fault, south of Grand Lake, western Newfoundland: preliminary results: Current Research – Newfoundland Department of Mines and Energy, Geological Survey Branch, Report, 02-1, p. 135–144.

—— 2003, Structural relationships south of Grand Lake, Newfoundland: Current Research – Newfoundland Department of Mines and Energy, Geological Survey Branch, Report, 03-1, p. 1–13.

Cawood, P. A., and van Gool, J. A. M., 1998, Geology of the Corner Brook - Glover Island region, Newfoundland: Geological Survey of Canada Bulletin 427, 96 p.

Cawood, P. A., Dunning, G. R., Lux, D., and van Gool, J. A. M., 1994, Timing of peak metamorphism and deformation along the Appalachian margin of Laurentia in Newfoundland: Silurian not Ordovician: Geology, v. 22, p. 399–402.

Cross, T. A., and Pilger, R. H., Jr., 1982, Controls of subduction geometry, location of magmatic arcs, and tectonics of arc and back-arc regions: Geological Society of America Bulletin, v. 93, p. 545–562.

Cumming, G. L., and Richards, J. R., 1975, Ore lead in a continuously changing Earth: Earth and Planetary Science Letters, v. 28, p. 55–171.

Currie, K. L., and van Berkel, J. T., 1992, Notes to accompany a geological map of the southern Long Range, southwestern Newfoundland: Geological Survey of Canada, Paper 91–10, 10 p.

Currie, K. L., van Breemen, O., Hunt, P. A., and van Berkel, J. T., 1992, Age of high-grade gneisses south of Grand Lake, Newfoundland: Atlantic Geology, v. 28, p. 153–161.

Davis, D. W., 1982, Optimum linear regression and error estimation applied to U-Pb data: Canadian Journal of Earth Sciences, v. 19, p. 2141–2149.

Dickin, A. P., and Raeside, R. P., 1990, Sm-Nd analysis of Grenville gneisses from Cape Breton Island, Nova Scotia: Proceedings of the LITHOPROBE-EAST Transect Meeting, St. John's, Newfoundland, p. 37–38.

Dubé, B., Dunning, G. R., Lauziere, K., and Roddick, J.C., 1996, New insights into the Appalachian Orogen from geology and geochronology along the Cape Ray fault zone, southwest Newfoundland: Geological Society of America Bulletin, v. 108, p. 101–116.

Dunning, G. R., Wilton, D. H. C., and Herd, R. K., 1989, Geology, geochemistry and geochronology of a taconic batholith, southwestern Newfoundland: Transactions of the Royal Society of Edinburgh: Earth Sciences, v. 80, p. 159–168.

Fox, D., and van Berkel, J. T., 1988, Mafic-ultramafic occurrences in metasedimentary rocks of southwestern Newfoundland: Geological Survey of Canada - Paper, v. 88-1B, p.41–48.

Goodwin, L. B., and Williams, P. F., 1990, Strike-slip movement along the Baie Verte Line, *in* Hall, J. editor, Lithoprobe Report, v. 13: Vancouver, Lithoprobe, p. 75–84.

—— 1996, Deformation path partitioning within a transpressive shear zone, Marble Cove, Newfoundland: Journal of Structural Geology, v. 18, p. 975–990.

Hall, L. A. F., and van Staal, C. R., 1999, Geology, southern end of Long Range Mountains (Dashwoods subzone), Newfoundland: Geological Survey of Canada, Open File 3727, scale 1:50,000.

Heaman, L. M., Erdmer, Ph., and Owen, J. V., 2002, U-Pb geochronologic constraints on the crustal evolution of the Long Range Inlier, Newfoundland: Canadian Journal of Earth Sciences, v. 39, p. 845–865.

Hibbard, J. P., 1983, Geology of the Baie Verte Peninsula, Newfoundland: Newfoundland Department of Mines and Energy, Mineral Development Division, Memoir 2, 279 p.

Hirth, G., and Tullis, J., 1992, Dislocation creep regimes in quartz aggregates: Journal of Structural Geology, v. 14, p. 145–159.

Hirth, G., Teyssier, C., and Dunlap, W. J., 2001, An evaluation of quartzite flow laws based on comparisons between experimentally and naturally derived rocks: International Journal of Earth Sciences, v. 90, p. 77–87.

Hyde, R. S., Miller, H. G., Hiscott, R. N., and Wright, J. A., 1988, Basin architecture and thermal maturation in the strike-slip Deer Lake Basin, Carboniferous of Newfoundland: Basin Research, v. 1, p. 85–105.

Jaffey, A. H., Flynn, K. F., Glendenin, L. E., Bentley, W. C., and Essling, A. M., 1971, Precision measurement of half-lives and specific activities of ^{235}U and ^{238}U: Physical Review C, v. 4, p. 1889–1906.

Jiang, D., and White, J. C., 1995, Kinematics of rock flow and the interpretation of geological structures with particular reference to shear zones: Journal of Structural Geology, v. 17, p. 1249–1265.

Krogh, T. E., 1973, A low-contamination method for hydrothermal decomposition of zircon and extraction of U and Pb for isotopic age determinations: Geochimica et Cosmochimica Acta, v. 37, p. 485–494.

—— 1982, Improved accuracy of U-Pb zircon ages by the creation of more concordant systems using an air abrasion technique: Geochimica et Cosmochimica Acta, v. 46, p. 637–649.

Lissenberg, C. J., Zagorevski, A., McNicoll, V. J., van Staal, C. R., and Whalen, J. B., 2005, Assembly of the Annieopsquatch Accretionary Tract, Newfoundland Appalachians: Age and geodynamic constraints from syn-kinematic intrusions: Journal of Geology, v. 113, p. 553–570.

Ludwig, K. R., 1998, On the treatment of concordant uranium-lead ages: Geochimica et Cosmchimica Acta, v. 62, p. 665–676.

—— 2001, User's manual for Isoplot/Ex rev. 2.49: a Geochronological Toolkit for Microsoft Excel: Special Publication, 1a, Berkeley Geochronology Center, Berkeley, 55 p.

McDougall, I., and Harrison, T. M., 1999, Geochronology and thermochronology by the ^{40}Ar/^{39}Ar method: New York, Oxford University Press, Inc., 269 p.

Miller, B. V., Dunning, G. R., Barr, S. M., Raeside, R. P., Jamieson, R. A., and Reynolds, P. H., 1996, Magmatism and metamoprhism in a Grenvillian fragment: U-Pb and ^{40}Ar/^{39}Ar ages from the Blair River Complex, northern Cape Breton Island, Nova Scotia, Canada: Geological Society of America Bulletin, v. 108, p. 127–140.

Passchier, C. W., and Trouw, R. A. J., 1996, Microtectonics: Berlin-Heidelberg, Springer Verlag, corrected 2nd printing, 289 p.

Pehrsson, S. J., van Staal, C. R., Herd, R. K., and McNicoll, V. J., 2003, The Cormacks Lake Complex, Dashwoods subzone; a window into the deeper levels of the Notre Dame Arc: Current Research – Newfoundland; Geological Survey Branch, Report, 03-1, p. 115–125.

Piasecki, M. A. J., 1988, Strain-induced mineral growth in ductile shear zones and a preliminary study of ductile shearing in western Newfoundland: Canadian Journal of Earth Sciences, v. 25, p. 2118–2129.

—— 1995, Dunnage Zone boundaries and some aspects of terrane development in Newfoundland, *in* Hibbard, J. P., van Staal, C. R., and Cawood, P. A., editors, Current Perspectives in the Appalachian-Caledonian Orogen: Geological Association of Canada, Special Paper 41, p. 323–347.

Piasecki, M. A. J., Williams, H., and Colman-Sadd, S. P., 1990, Tectonic relationships along the Meelpaeg, Burgeo, and Burlington Lithoprobe transects in Newfoundland: Current Research – Newfoundland, Geological Survey Branch, Report, 90-1, p. 327–339.

Pryer, L. L., 1993, Microstructures in feldspars from a major crustal thrust zone: the Grenville Front, Ontario, Canada: Journal of Structural Geology, v. 15, p. 21–36.

Renne, P. R., Deino, A. L., Walter, R. C., Turrin, B. D., Swisher, C. C., Becker, T. A., Curtis, G. H., Sharp, W. D., and Jaouni, A. R., 1994, Intercalibration of astronomical and radioisotopic time: Geology, v. 22, p. 783–786.

Roddick, J. C., 1983, High-precision intercalibration of ^{40}Ar/^{39}Ar standards: Geochimica et Cosmochimica Acta, v. 47, p. 887–898.

—— 1988, The assessment of errors in ^{40}Ar/^{39}Ar dating: *in* Radiogenic Age and Isotopic Studies, Report 2: Geological Survey of Canada, Paper 88-2, p. 7–16.

Roddick, J. C., Cliff, R. A., and Rex, D. C., 1980, The evolution of excess argon in alpine biotites; a ^{40}Ar/^{39}Ar analysis: Earth and Planetary Science Letters, v. 48, p. 185–208.

Sacks, P. E., Malo, M., Trzcienski, W. E., Jr., Pincivy, A., and Gosselin, P., 2004, Taconian and Acadian transpression between the internal Humber Zone and the Gaspé Belt in the Gaspé Peninsula: tectonic history of the Shickshock Sud fault zone: Canadian Journal of Earth Sciences, v. 41, p. 635–653.

Scaillet, S., 2000, Numerical error analysis in ^{40}Ar/^{39}Ar dating: Chemical Geology, v.162, p. 269–298.

Stern, R. A., 1997, The GSC Sensitive High Resolution Ion Microprobe (SHRIMP): analytical techniques of zircon U-Th-Pb age determinations and performance evaluation, *in* Radiogenic Age and Isotopic Studies, Report 10: Geological Survey of Canada, Current Research 1997-F, p. 1–31.

Stern, R. A., and Amelin, Y., 2003, Assessment of errors in SIMS zircon U-Pb geochronology using a natural zircon standard and NIST SRM 610 glass: Chemical Geology, v. 197, p. 111–146.

van der Velden, A. J., van Staal, C. R., and Cook, F. A., 2004, Crustal structure, fossil subduction, and the tectonic evolution of the Newfoundland Appalachians: evidence from a reprocessed seismic reflection survey: Geological Society of America Bulletin, v. 116, p. 1485–1498.

van Staal, C. R., 2007, Pre-Carboniferous tectonic evolution and metallogeny of the Canadian Appalachians, *in* Goodfellow, W. D., editor, Mineral Resources of Canada: A Synthesis of Major Deposit-types, District Metallogeny, the Evolution of Geological Provinces, and Exploration Methods: Mineral Deposit Division, Geological Association of Canada, Special Publication 5.

van Staal, C. R., Dewey, J. F., MacNiocaill, C., and McKerrow, W. S., 1998, The Cambrian-Silurian tectonic evolution of the northern Appalachians and British Caledonides: history of a complex west and southwest Pacific-type segment of Iapetus, *in* Blundell, D., and Scott, A. C., editors, Lyell; the past is the key to the present: Geological Society Special Publication 143, p. 199–242.

van Staal, C. R., Whalen, J. B., McNicoll, V. J., Pehrsson, S., Lissenberg, C. J., Zagorevski, A., van Breemen, O., and Jenner, G. A., 2007, The Notre Dame Arc and the Taconic Orogeny in Newfoundland, *in* Hatcher, R. D., Jr., Carlson, M. P., McBride, J. H., and Martínez Catalán, J. R., editors, Four-D Framework of Continental Crust: Geological Society of America Memoir 200, doi: 10.1130/2007.1200(26).

Villeneuve, M. E., and MacIntyre, D. G., 1997, Laser ^{40}Ar/^{39}Ar ages of the Babine porphyries and Newman Volcanics, Fulton Lake map area, west-central British Columbia, *in* Radiogenic Age and Isotopic Studies, Report 10: Geological Survey of Canada, Current Research 1997-F, p.131–139.

Villeneuve, M. E., Sandeman, H. A., and Davis, W. J., 2000, A method for the intercalibration of U-Th-Pb and ^{40}Ar/^{39}Ar ages in the Phanerozoic: Geochimica et Cosmochimica Acta, v. 64, p. 4017–4030.

Waldron, J. W. F., and van Staal, C. R., 2001, Taconian Orogeny and the accretion of the Dashwoods Block; a peri-Laurentian microcontinent in the Iapetus Ocean: Geology, v. 29, p. 811–814.

Whalen, J. B., and Currie, K. L., 1983, The Topsails igneous terrane of western Newfoundland: Current Research Part A- Geological Survey of Canada, Paper 83-1A, p. 15–23.

Whalen, J. B., Currie, K. L., and van Breemen, O., 1987, Episodic Ordovician - Silurian plutonism in the Topsails igneous terrane, western Newfoundland: Transactions of the Royal Society of Edinburgh: Earth Sciences, v. 78, p. 17–28.

Whalen, J. B., Currie, K. L., and Piasecki, M. A. J., 1993, A re-examination of relationships between Dunnage subzones in southwest Newfoundland: Current Research Part D: Geological Survey of Canada, Paper 93-1D, p. 65–72.

Whalen, J. B., Jenner, G. A., Longstaffe, F. J., Gariépy, C., and Fryer, B. J., 1997, Implications of granitoid geochemical and isotopic (Nd, O, Pb) data from the Cambrian-Ordovician Notre Dame arc for the evolution of the Central Mobile belt, Newfoundland Appalachians, *in* Sinha, K., Whalen, J. B., and Hogan, J. P., editors, The Nature of Magmatism in the Appalachian Orogen: Geological Society of America Memoir 191, p. 367–395.

Whalen, J. B., McNicoll, V. J., van Staal, C. R., Lissenberg, C. J., Longstaffe, F. J., Jenner, G. A., and van Breeman, O., 2006, Spatial, temporal and geochemical characteristics of Silurian collision-zone magmatism: an example of a rapidly evolving magmatic system related to slab break-off: Lithos, v. 89, p. 377–404.

Williams, H., editor, 1995, Geology of the Appalachian-Caledonian orogen in Canada and Greenland: Geological Survey of Canada, Geology of Canada, no. 6 (also Geological Society of America, The Geology of North America, v. F1), 944 p.

Williams, H., and St-Julien, P., 1982, The Baie Verte-Brompton Line; early Paleozoic continent-ocean interface in the Canadian Appalachians, *in* St-Julien, P., and Beland, J. editors, Major structural zones and faults of the Northern Appalachians: Geological Association of Canada, Special Paper 24, p. 177–208.

Williams, H., Colman-Sadd, S. P., and Swinden, H. S., 1988, Tectonic-stratigraphic subdivisions of central Newfoundland: Geological Survey of Canada Paper 88-1B, Current research Part B, p. 91–98.

Williams, S. H., 1992, Lower Ordovician (Arenig-Llanvirn) graptolites from the Notre dame Subzone, central Newfoundland: Canadian Journal of Earth Sciences, v. 29, p. 1717–1733.

Wilson, T., 1962, Cabot Fault, an Appalachian equivalent of the San Andreas and Great Glen Fault and some implications for continental displacement: Nature, v. 195, p. 135–138.

Zagorevski, A., Rogers, N., van Staal, C. R., McNicoll, V., Lissenberg, C. J., and Valverde-Vaquero, P., 2006, Lower to Middle Ordovician evolution of peri-Laurentian arc and back-arc complexes in the Iapetus: constraints from the Annieopsquotch Accretionary Tract, Central Newfoundland: Geological Society of America Bulletin, v. 118, p. 324–342.